DEPARTMENT OF THE AIR FORCE

AIR UNIVERSITY

AIR FORCE INSTITUTE OF TECHNOLOGY

Wright-Patterson Air Force Base, Ohio

AFIT/GNE/ENP/91M-6

HIGH ALTITUDE NEUTRAL PARTICLE TRANSPORT USING THE MONTE CARLO SIMULATION CODE MCNP WITH VARIABLE DENSITY ATMOSPHERE

THESIS

David L. Monti
Captain, USAF

AFIT/GNE/ENP/91M-6

Approved for public release; distribution unlimited

AFIT/GNE/ENP/91M-6

HIGH ALTITUDE NEUTRAL PARTICLE TRANSPORT USING THE MONTE CARLO SIMULATION CODE MCNP WITH VARIABLE DENSITY ATMOSPHERE

THESIS

Presented to the Faculty of the School of Engineering

of the Air Force Institute of Technology

Air University

In Partial Fulfillment of the

Requirements for the Degree of

Master of Science in Nuclear Engineering

David L. Monti, B.S.

Captain, USAF

March 1991

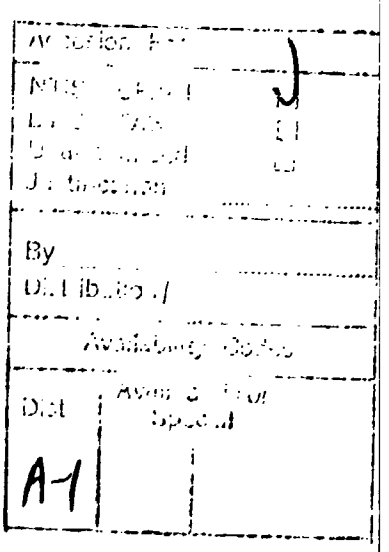

Approved for public release; distribution unlimited

Preface

The purpose of this study was to perform Monte Carlo simulations of neutral particle transport with primary and secondary photon production as it applies to a point isotropic source within a variable density atmosphere. Specifically, the goal was to increase the accuracy of neutral particle transport calculations within the atmosphere by accurately representing the variability of air density with altitude. During this study, analytic representations for air density and mass integral, which modelled the variation of air density with altitude, were developed. The generalized Monte Carlo code MCNP required modification using the newly developed atmospheric model. The modifications were thoroughly tested before actual real world simulation studies were performed.

Guidance and support for this effort was received from many sources. First, I would like to thank my thesis advisor LCDR Kirk A. Mathews. His expertise in the field of radiation transport proved to be invaluable in enhancing the success of my project. Second, I would like to thank the members of my thesis committee; Capt. Mike Sabochik and Maj. Denis Beller for their assistance in the preparation of the final copy of this thesis. I would also like to thank Judy Briestmeister and Tom Booth from Los Alamos National Laboratory for their assistance with MCNP. Finally, I would like to thank my wife, Tina and daughter, Nina for their unending

patience and support.

David L. Monti

Table of Contents

	Page
Preface	ii
List of Figures	vi
List of Tables	vii
Abstract	viii
Executive Summary	x
I. Introduction	1
Background	1
Problem	3
General Approach	4
Scope of the Project	5
Assumptions	6
Sequence of Presentation	6
II. Theoretical Development	8
Introduction	8
Density Variation of the Atmosphere	8
Modelling the Density Variation	11
Computing the Integrated Mass Density	13
Mass-Integral Scaling (MIS)	17
III. MCNP and SMAUG-II Code Descriptions	23
MCNP Code	23
SMAUG-II Code	23
IV. MCNP Modifications	26
Transport Program Flow	26
Reference Density	28
Transport Parameters	29
Auxiliary Modifications	40
V. MCNP Input Parameters	42
Problem Geometry	42
Source Spectra	45
Material Specifications	47
Variance Reduction	47
Cross-Sections	48
Tallies	50

VI. Results and Discussion 52

Introduction 52
Validation of MCNP Modifications 52
MCNP and SMAUG-II Results 58

VII. Summary and Conclusions 79

Summary 79
Conclusions 80

VIII. Recommendations 85

Appendix A: 86

Appendix B: 93

Appendix C: 95

Appendix D: 98

Appendix E: 103

Appendix F: 112

Bibliography 115

Vita 116

List of Figures

		Page
1.	Density vs. Geometric Altitude from the U.S. Standard Atmosphere Tables, 1976	9
2.	Cumulative Mass Integral as a Function of Geometric Altitude for a Polar Angle of 0 Degrees	16
3.	Source-Detector Geometry	21
4.	Spatial Cell Geometry for Co-Altitude Detectors	44
5.	MCNP vs. SMAUG Neutron Fluence at Source Co-Altitude vs. Range (Slant Range)	59
6.	MCNP vs. SMAUG Neutron Fluence at Source Co-Altitude vs. Mass-Integral	60
7.	MCNP vs. SMAUG Photon Fluence at Source Co-Altitude vs. Radius (Slant Range)	65
8.	MCNP vs. SMAUG Photon Fluence at Source Co-Altitude vs. Mass-Integral	66
9.	Ratio of SMAUG to MCNP Neutron Fluence for Short Ranges vs. Angle	71
10.	Ratio of SMAUG to MCNP Photon Fluence at Short Ranges vs. Angle	74

List of Tables

		Page
1.	Mean Free Path for a 2 MeV Neutron vs. Altitude	10
2.	Atmospheric Parameters for Constant Density Scale Height Regions	12
3.	Atmospheric Parameters for Constant Mass-Integral Scale Height Regions	18
4.	Ratio of SMAUG to MCNP Neutron Fluence at Source Co-Altitude versus Range	62
5.	Ratio of SMAUG to MCNP Photon Fluence at Source Co-Altitude versus Range	68

Abstract

The generalized Monte Carlo transport code, MCNP was modified for purposes of two-dimensional neutron-photon transport modelling in a variable density atmosphere. Calculations were performed using cylindrical (r,z) geometry and a point isotropic neutron-photon source at a source altitude of 40 kilometers. Geometrical dimensions of the problem were large, approaching 90,000 square kilometers. A collection of neutron-photon fluence results using ring detectors were computed for field points at constant ranges as a function of source elevation angle and for field points at constant altitudes as a function of radius. These results may be useful to others as benchmark results for further studies using discrete ordinates. Results showed a decrease in run time by a factor of two was possible using the modified version of MCNP. The run time comparison was based on a study performed by Culp et al. using the unmodified MCNP code. Only a fraction of the spatial cells required in the study by Culp et al. were used. Results showed streaming of the neutron and photon radiation at very close ranges. Buildup from multiple scattering contributions proved to be the dominant effect at intermediate ranges. Attenuation from successive downscatter in energy was shown to be the dominant effect at ranges greater than about 60 kilometers. Results

indicated neutrons to be the dominant form of radiation based on the magnitude of the fluences. Results obtained with MCNP were compared to those obtained with the computer code SMAUG-II, which uses the mass-integral scaling approximation. The comparison showed SMAUG-II to be fairly accurate at points close to the source, but severe errors were encountered at ranges exceeding about 9 kilometers for points at or above the source altitude.

Executive Summary

Introduction

Computers have become increasingly powerful in recent years, making two-dimensional Monte Carlo transport studies more affordable. Because the density of air varies approximately exponentially with altitude, there is a need to incorporate an efficient, sophisticated method to represent this density variation as an alternative to using a constant scale height spatial mesh. In a constant scale height spatial mesh, large numbers of discrete cells are used to represent the variation of air density with altitude. Assuming exponential behavior, a constant scale height factor ("e-fold" distance) was used to compute the density within each region. This large proliferation of cells imposed limitations on the size of the geometry; computer run time was increased as a consequence of using a large number of cells.

If a variable density atmospheric model can be implemented into a production Monte Carlo transport code, an improvement in the overall accuracy over previously used schemes can be achieved. An increase in the geometrical dimensions of the problem and a decrease in run time would be an added benefit of this density model.

A four-phase approach was used to develop, test, and run the modified MCNP code:

1) analytic functions were developed to represent both the density variation and cumulative mass-integral as a function of altitude based on data extracted from the U.S. Standard Atmosphere Tables, 1976;

2) the fitting functions were implemented into MCNP and the necessary auxiliary modifications were accomplished;

3) the accuracy of the MCNP modifications were validated by running a series of Monte Carlo simulations. Results were compared to those obtained using the unmodified version of MCNP;

4) High altitude Monte Carlo neutron-photon simulation studies were performed using the modified MCNP code for a variety of test cases.

The following assumptions and approximations were used in performing the transport simulations:

1) the molecular constituents of the atmosphere consisted only of nitrogen, oxygen, and argon which normally make up 99.9 percent of the atmosphere;

2) the fractional composition of the air remained constant as a function of altitude;

3) there was no time dependence in the analysis;

4) the source was modelled as a point isotropic neutron-photon source;

5) the variation of air density with altitude was represented by a series of continuous piecewise e nential interpolating curves.

Theoretical Development

For this study, analytic functions were developed to represent the approximately exponential variation of air density with altitude and the cumulative mass-integral as a function of altitude. These expressions are given by equations (2) and (6), respectively. The atmosphere from ground level up to an altitude of 1000 kilometers was divided up into 36 scale height regions. The density variation within each scale height region was represented using an exponential function. Each exponential function used a different density scale height factor to represent the change in air density over the scale height region. Density scale height factors for each region were computed by fitting a table of reference density values using an iterative solver routine employing Newton's method. Mass-integral data were computed by integrating a table of reference density values using a Simpson's 1/3 Rule numerical integration routine. The data was then tabulated as cumulative distribution of mass-integral versus altitude. The mass-integral scale height factors for each region were then computed using the same iterative solver. A total of 72 scale height factors were computed to 16-digit precision to enhance the accuracy.

Equation (2) computes air density and equation (6) computes cumulative mass-integral as a function of geometric altitude given the appropriate scale height factors. Equations (3) and (7) represent the inverted forms of equations

(2) and (6), respectively. Equation (3) computes an altitude given an air density and equation (7) computes an altitude given a mass-integral. These four expressions, together with the scale height factors, the corresponding base altitudes, the densities, and the mass-integrals, completes the atmospheric density model. The 36 atmospheric regions together with the parameters for density and mass-integral are tabulated in Tables 2 and 3, respectively.

As an alternative to Monte Carlo computational modelling of neutron-photon transport, faster computer codes utilizing the mass-integral scaling approximation are used. Mass-integral scaling involves approximating the fluence or dose in a variable density system with previously computed results of fluence or dose in a homogeneous system. The results are based on discrete ordinates numerical solutions to the Boltzmann transport equation for an infinite homogeneous system. These results are then extended to a variable density system by using the scaling laws given by equations (8) and (9) for a cylindrical (r,z) geometry. Since air density varies with altitude, z, the mass-integral can be found from equation (10). This expression states that the mass-integral is a function of altitude, density, and the source elevation angle ("look" angle). The geometry is shown in figure 3.

The computer code SMAUG-II, based on mass-integral scaling, relies upon discrete ordinates calculations of neutron and photon transport in a homogeneous medium.

The discrete ordinates results are based on a set of least-squares fits obtained from the computer code ANISN, a one-dimensional discrete ordinates code.

Results and Discussion

Validation of the modified MCNP code showed good agreement as compared to unmodified MCNP results. Comparison results showed relative differences of approximately 2 percent when using a large number of coarse spatial cells in the unmodified version of MCNP. Relative differences of 1 percent or less were achieved when fine-mesh spatial grids with accurate average densities in each scale height region were used. Note that the unmodified MCNP code, using a constant density spatial mesh, produced results that were within 2 percent of the continuously variable air density model. However, a very large number of cells were required in the unmodified MCNP code. The region of comparison in this case was restricted to radii not exceeding 100 km because of the excessive run time required.

Two basic simulation scenarios were used in performing the Monte Carlo transport studies. The first involved computing neutron and photon fluence values using ring detectors at the source altitude of 40 kilometers. The second scenario involved calculating neutron and photon fluence values using ring detectors at constant ranges as a function of source elevation angle. Ring detectors are usually necessary when there are few scattering events near the point of interest.

Ring detectors are useful when there is at least one degree of symmetry about a coordinate axis, in this case, the z-axis. The computer code SMAUG-II was then used to generate results for the same field point locations for comparison purposes.

Fluence data computed using MCNP behaved in an anticipated manner, offering no particular surprises. The magnitude of the neutron fluence was shown to be roughly an order of magnitude higher than the corresponding photon results. This indicated that neutrons were the principal form of radiation in this analysis. This also implied that the mean free path for neutron scatter was short compared to that for photons.

Along the source co-altitude band, streaming of the neutron and photon radiation was observed, indicating reduced scatter contributions at very short ranges and low mass-integral. For both neutron and photon radiation, buildup at intermediate ranges from multiple scattering contributions increased for decreasing source elevation angle and increasing range. The amount of buildup from the photon radiation was less pronounced than that from the neutron radiation. At long ranges, attenuation of the neutron radiation, due to successive downscatter and diffusion away from the points of interest, began to dominate over buildup. For the photon data, attenuation from successive scatter and absorption at low photon energies

dominated buildup at longer ranges. From 3 kilometers out to at least 250 kilometers, the primary photon radiation was the principal contributor to the total coupled photon free-field fluence. Results indicated that the secondary photon radiation became prominent at very long ranges, and converged towards secular equilibrium with the neutron radiation. This served as evidence that the neutron radiation acted as a source for the secondary photon radiation.

With respect to the approximations used in this analysis, SMAUG-II predictions of neutron-photon transport characteristics were shown to be accurate to within a few percent at points within a few kilometers of the source. SMAUG-II had the greatest difficulty in predicting the fluence in regions of higher density and over large mass ranges.

Based on comparison results with MCNP, there were several deficiencies noted with SMAUG-II. First, SMAUG-II could not account for the escape of particles from the problem, especially out the top. Second, SMAUG-II is inadequate for use at altitudes above the original 20 kilometer limit. This stems from the inability of SMAUG-II to account for multidimensional transport effects such as buildup, downscatter, etc. inherent in a variable density atmosphere. This severely limits the usefulness of SMAUG-II as an initial transport diagnostic tool or as a tool for comparison against other radiation transport methods.

Increasing the geometrical dimensions of the problem

over previously used geometries in past Monte Carlo studies was now possible. The increase in run time as a consequence of incorporating a variable density atmosphere into MCNP was more than offset by the time saved in eliminating unneeded spatial cells to represent the variation of air density with altitude. An added benefit was to decrease some of the user overhead in preparing the input files.

In terms of computational costs, using ring detectors proved to be very expensive in comparison to cell or surface tallies. However, ring detectors were necessary because large cells were often used in the problem geometry, rendering the use of cell or surface tallies meaningless.

In comparison to run times obtained using an unmodified version of MCNP, run times from the modified version of MCNP proved to be extremely favorable. The number of cells required was substantially reduced, and as a consequence, the overall run time was reduced and the problem dimensions could be increased.

SMAUG-II and MCNP neutron fluence results for the first scenario are shown graphically in figures 5 and 6. Comparison results between SMAUG-II and MCNP are listed in Table 4. Photon fluence results are shown in figures 7 and 8. Comparison results are given in Table 5. SMAUG-II and MCNP neutron and photon comparison results for the second scenario are shown as polar plots in figures 9 and 10, respectively.

Summary and Conclusions

The above results were influenced by several factors. First, the mean free path for neutron scatter was short compared to that for photons, making neutrons the dominant form of radiation in this analysis. Second, results showed that secondary photon transport was directly coupled with neutron transport, and the photon radiation became increasingly important as range increased. Also, the primary photon radiation was the primary contributor to the total photon free-field fluence. Third, scattering was the dominant transport mechanism for both neutrons and photons.

Recommendations

Five specific recommendations for furtner study in this area are made. First, develop the modified MCNP code so that it is applicable to a wider variety of density-dependent transport problems. Second, investigate alternate geometries and/or variance reduction schemes to increase the efficiency of transport simulations. Third, alternative array-search algorithms might improve the efficiency of the modified MCNP code. Fourth, MCNP should be further modified to allow the use of multiple materials within the atmosphere. Finally, modifications to allow the user to select either the variable density version or the unmodified version should be incorporated into a single code.

HIGH ALTITUDE NEUTRAL PARTICLE TRANSPORT USING THE MONTE CARLO SIMULATION CODE MCNP WITH VARIABLE DENSITY ATMOSPHERE

I. Introduction

Background

The most widely used method today for representing the variation of air density in Monte Carlo transport calculations is to use spatial cells, where the density within each cell is constant. The variation of air density with altitude was then represented using a series of constant density regions.

Past studies performed by Shulstad [1] in 1976 and Culp, Monti, Shoemaker, Wesley, and Mathews [2] in 1990 have investigated different methods for incorporating a variable density atmosphere in order to perform atmospheric transport calculations. In response to a growing need for faster running computer codes for solving transport problems in the 1970's, Shulstad developed a specialized multigroup diffusion code on a two-dimensional non-orthogonal coordinate system. Mass-integral scaling was incorporated into this coordinate system in order to model the approximately exponential variation of air density with altitude. Shulstad's efforts were successful, but were limited in accuracy by the assumption of isotropic or at most linear isotropic scat-

tering. Reasonable accuracy was obtained only if the mean free path of the particle was short relative to the distance over which the density varied significantly.

The advent of powerful computers in the 1980's and 1990's allowed for solving the transport problem using a two-dimensional Monte Carlo analysis. The study performed by Culp et al. involved solving the transport problem of a point isotropic source at high altitude (40 km) using Monte Carlo techniques. The study assumed an exponential atmosphere and approximated the variation of air density with altitude by using a series of piecewise-constant spatial grids to represent $\rho(z)$. The equation used to represent this density variation is shown below.

$$\rho = \rho_0 \exp\left[\frac{(-(z_{(i+1)}+z_i)/2)}{7}\right] \qquad (1)$$

where

$\rho(z_i)$ = air density at lower region of i^{th} altitude band [g/cm^3]

$\rho(z_{i+1})$ = air density at upper region of i^{th} altitude band [g/cm^3]

z_{i+1} = upper altitude of i^{th} region [km]

z_i = lower altitude of i^{th} region [km]

The 7 km scale height factor used in equation (1) represented the vertical distance required for the air density to decrease by a factor of e. This method had limitations

because in the real case the atmospheric density cannot be represented by using constant density altitude bands which use a single constant density scale height factor. A continuously variable exponential function within each region, each with a characteristic scale height factor, would be more accurate for representing the variation of air density as a function of altitude.

The primary emphasis of the study by Culp et al. centered on comparing mass-integral scaling results from the computer code SMAUG-II [3] to Monte Carlo results from MCNP [4]. Results showed that mass-integral scaling overestimated the radiation at high altitudes and at long ranges. [2:30]

Problem

Past studies have shown that mass-integral scaling is only correct when applied to a uniform homogeneous medium, but is an approximation in the real case. Likewise, Monte Carlo calculations using a constant density spatial grid throughout the problem is also only an approximation to the real case.

Because computers have become increasingly powerful, multidimensional computational modelling of neutral particle transport within the atmosphere has become much more affordable. There is a need to incorporate a more sophisticated variable density atmosphere as an alternative to using a simple constant scale height spatial mesh or a mass-integral scaling approximation.

Once a variable density capability has been incorporated into a working production Monte Carlo code, an improvement in overall accuracy previously afforded by using other atmospheric modelling techniques in studying the transport problem will be possible.

General Approach

High altitude neutron-photon transport studies within a variable density atmosphere were based on a four phase approach as given below.

1) Develop analytic functions for obtaining both density and integrated mass density (mass-integral) values. There are two functional forms for the analytical expressions, one for density and one for mass-integral. These expressions can be derived by fitting these functions directly to a sufficiently dense table of atmospheric density values obtained from the U.S. Standard Atmosphere Tables, 1976 [5] and forming a grid of density and mass- integral scale height factors.

2) Implement the fitting functions into the Monte Carlo code MCNP and accomplish the necessary auxiliary modifications in order to use the derived analytic functions and the scale height factors.

3) Validate the accuracy of the atmospheric model by running simple one-dimensional test cases or use simple input files which incorporate a fine spatial grid with accurate average densities in each scale height region. Compare

results to those obtained with the variable density atmospheric model.

4) Perform Monte Carlo simulation studies of neutron-photon transport within a variable density exponential atmosphere using a point isotropic source at high altitudes (40 km) and study the effects over high mass ranges ($\geq$ 100 g/cm^2). Compare MCNP results to those obtained with SMAUG-II.

Scope of the Project

This study involved the development of analytic representations for air density and mass-integral which modelled the approximately exponential variation of air density with altitude. The generalized Monte Carlo code MCNP required modification so that, at minimum, it was applicable to any type of radiation transport study within a variable density atmosphere, with some exceptions. These exceptions are explained in section IV. Specifically the above methods were used to generate a collection of benchmark results for a single source altitude at selected field points (detectors) for two scenarios: 1) constant range versus source elevation angle and 2) field point altitude bands versus range. Results for the regions of interest were mapped out in a multidimensional fashion giving fluence distribution values for both range and angle. Fluence results obtained with MCNP were then compared to those obtained with SMAUG-II. These results can be used as benchmarks for other transport tech-

niques such as discrete ordinates.

Assumptions

In order to prevent unneeded computational complexity which would have little effect on accuracy, the following assumptions were made:

1) The atmospheric gas (molecular) constituents consisted only of nitrogen, oxygen, and argon which normally make up 99.9 percent of the atmosphere;

2) The fractional composition of the atmosphere was not a function of altitude;

3) There is no time dependence in the problem, only fluence calculations were considered;

4) The source was modelled as a point isotropic neutron-photon source. The default spectra from the SMAUG-II code was used to facilitate the comparison between MCNP and SMAUG-II;

5) The variation of air density with altitude was modelled by using continuous piecewise exponential curves in each scale height region.

Sequence of Presentation

Section II presents a detailed discussion of how the atmospheric model was derived and the sources of data used. Section III provides a general description of the computer codes used in this analysis, MCNP and SMAUG-II. Section IV addresses the MCNP code modifications and their implemen-

tation. Section V discusses the input parameters used in the MCNP code, i.e., problem geometry, materials used, selection of tallies, variance reduction techniques, and cross section tables. Section VI presents the results and discussion of the Monte Carlo simulations as it applies to the modifications built into MCNP. Section VI also presents the methods used to valicate the MCNP modifications. Summary and conclusions are presented in section VII, which are drawn directly from results obtained in section VI. Section VIII makes recommendations for future work in this area.

II. Theoretical Development

Introduction

Section I explained some of the basic concepts of a variable density exponential atmosphere, and the steps necessary to represent the density variation of air with altitude. Section I also presented the basic scope and the assumptions used in this study. This section will present the theoretical development used in representing the variable density atmosphere and a theoretical discussion of mass-integral scaling. Topics discussed include: the source of atmospheric data, analytic forms of the density and mass-integral equations and the determination of scale height factors for both density and mass-integral.

Density Variation of the Atmosphere

The variation of air density with altitude is approximately exponential, that is, density decreases exponentially with increasing altitude up to about 110 kilometers. This behavior is shown in figure 1. The exponential nature of the air density versus altitude is evident up to an altitude of approximately 110 km. Above this altitude, the data begins to deviate somewhat from a true exponential. The data used in figure 1 was obtained from the U.S. Standard Atmosphere Tables, 1976 [5:50-73].

In order to solve transp... problems within the atmosphere, it was necessary to represent this density variation

as accurately as possible without greatly increasing the computational work.

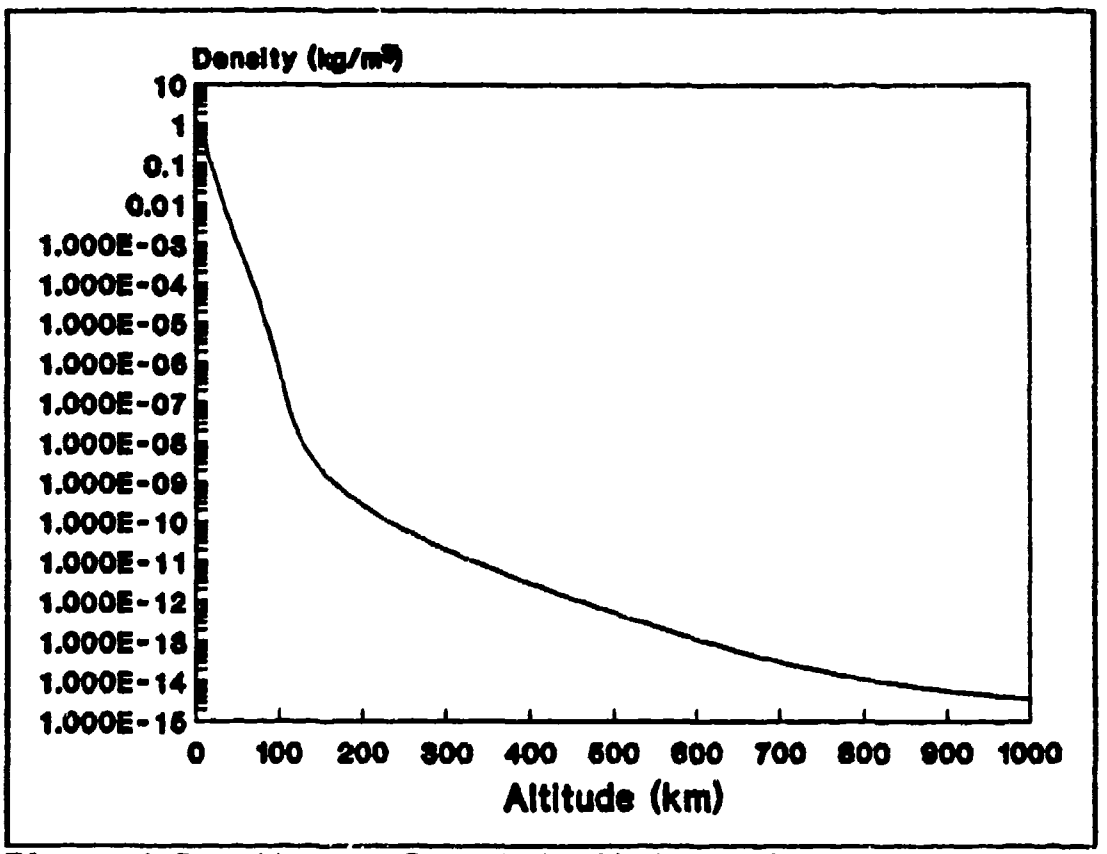

Figure 1 Density vs. Geometric Altitude from the U.S. Standard Atmosphere Tables, 1976.

For early development work of the atmospheric model, an altitude limit of 1000 km was imposed because of the 1000 km limit in the 1976 data tables [5:50-73]. In performing the actual Monte Carlo calculations, considerable computer time can be saved by cutting the effective "top of the atmosphere" down to an altitude where there is much less than one mean free path of atmosphere remaining for either neutrons or photons. Above this altitude, the probability for interac-

tion is very small. It is often necessary to tailor the limit of the "sensible" atmosphere to a specific problem, where high altitude detectors might be used.

Table 1 lists the mean free path versus altitude and density for a 2 MeV neutron, the average energy in the spectrum used here. It is clear that at about 70 km, there is less than one mean free path for neutrons remaining within the defined atmosphere. There is a certain probability that contributions from particles that scatter downward from collisions between the specified altitude limit and the 70 km suggested limit might be missed. Because of this, significant error could result if a Monte Carlo analysis is performed using an upper altitude of less than 70 km.

Table 1: Mean Free Path for a 2 MeV Neutron vs. Altitude

Altitude [km]	Density [g/cm³]	MFP [cm] / [km]
Sea Level	1.2250E-3	1.23E+4 / 0.123
10.0	4.1351E-4	3.63E+4 / 0.363
20.0	8.8910E-5	1.69E+5 / 1.69
60.0	3.0968E-7	4.85E+7 / 485
70.0	8.2829E-8	1.81E+8 / 1810
80.0	1.8458E-8	8.14E+8 / 8140
90.0	3.4160E-9	4.40E+9 / 44000
100.0	5.6040E-10	2.68E+10 / 268000
150.0	2.0760E-12	7.24E+12 / 7.24E+7
200.0	2.5410E-13	5.91E+13 / 5.91E+8

Modelling the Density Variation

If the variation of air density is approximated as piecewise exponential and the "sensible" atmosphere is divided up into vertical regions for increased accuracy, then curve-fits for the density variation have the following mathematical form (for $z_i \leq z < z_{i+1}$)

$$\rho(z) = \rho(z_i) \exp\left[-\frac{(z-z_i)}{B_i}\right] \qquad (2)$$

where

$\rho(z)$ = density at specified altitude [g/cm^3]

$\rho(z_i)$ = density at base altitude of i^{th} region [g/cm^3]

z = specified altitude [cm]

z_i = base altitude of i^{th} region [cm]

S_i = density scale height factor of i^{th} region [cm]

The parameters needed in equation (2) to calculate density up to a maximum altitude of 990 km are presented in Table 2. Inverting equation (2) results in the following expression which calculates the altitude for a given density (for $\rho(z_i) \geq \rho(z) > \rho(z_{i+1})$)

$$z = z_i - S_i LN[\rho(z)/\rho(z_i)] \qquad (3)$$

Density values were taken directly from the U.S. Standard Atmosphere Tables, 1976 [5:50-73]. To obtain good accuracy, the atmosphere was partitioned into 36 scale height regions. TK Solver Plus was used to calculate a density scale height

factor for each region by forcing

$$\rho(z_{(i+1)}) = \rho(z_i) \exp\left[-\frac{(z_{(i+1)} - z_i)}{S_i}\right] \qquad (4)$$

given z_i, z_{i+1}, ρ_i, and ρ_{i+1} to determine S_i. An iterative solver algorithm using Newton's method was used for this purpose. The 36 atmospheric regions together with the corresponding parameters for density are presented in Table 2.

Table 2: Atmospheric Parameters for Constant Density Scale Height Regions

Region	Z_L [km]	Z_H [km]	ρ_i [kg/m^3]	S_i [km]
1	0	1	1.225	10.30391726068488
2	1	2	1.1117	10.06927055016300
3	2	3	1.0066	9.83153560749636
4	3	4	9.0925E-1	9.60534141126499
5	4	5	8.1935E-1	9.37232106253662
6	5	10	7.3643E-1	8.66352196902309
7	10	15	4.1351E-1	6.64086763389816
8	15	20	1.9476E-1	6.3763846529
9	20	25	8.8910E-2	6.27630265119
10	25	30	4.0084E-2	6.426047540969
11	30	40	1.8410E-2	6.545893995756
12	40	50	3.9957E-3	7.36011605750619
13	50	60	1.0269E-3	8.34195106975831
14	60	70	3.0968E-4	7.58287361663704
15	70	80	8.2829E-5	6.66098102745308
16	80	90	1.8458E-5	5.92758528126849
17	90	100	3.4160E-6	5.53227469727463
18	100	110	5.6040E-7	5.70413094786334
19	110	120	9.7080E-7	6.78176406889826
20	120	130	2.2220E-8	9.97277941535646

Table 2: (Continued)

Region	Z_L [km]	Z_H [km]	ρ_i [kg/m^3]	S_i [km]
21	130	140	8.1520E-9	13.2426226009301
22	140	150	3.8310E-9	16.3216567546257
23	150	160	2.0760E-9	19.194125389299
24	160	180	1.2330E-9	23.1339249629764
25	180	200	5.1940E-10	27.9741247049562
26	200	240	2.5410E-10	34.0828528670665
27	240	280	7.8580E-11	41.1254588557962
28	280	320	2.9710E-11	46.8045755271109
29	320	400	1.2640E-11	53.1146385350911
30	400	480	2.8030E-12	58.9065250294756
31	480	560	7.2080E-13	63.6011115831811
32	560	640	2.0490E-13	69.8932556471199
33	640	720	6.5230E-14	81.6274032394408
34	720	800	2.4480E-14	104.199494345468
35	800	880	1.1360E-14	141.881682961411
36	860	990	6.4640E-15	198.699242408463

In Table 2, the column headed 'Region' contains the region number, i, the column headed 'Z_L' contain values of z_i, and the column headed 'Z_H' contain values of z_{i+1}.

The density scale height factors, the base altitudes of the regions, and the air densities at the base altitudes were tabulated as table look-up values and loaded into arrays. See Section IV, "Auxiliary Modifications", for more information.

Computing the Integrated Mass Density

In order to perform transport calculations in a variable density atmosphere, it was necessary to create a table of integrated mass density (mass-integral) values as a function

of altitude. It was then necessary to derive a mathematical formula which calculated a mass-integral between any two points in space lying on a vertical line. A correction for points which do not lie on a vertical line is made by dividing the mass-integral by the vertical, or z-direction cosine, using the polar angle as a reference. A Microsoft QuickBasic program, INTEG_MI.BAS, was written which calculated the mass-integral by integrating the table of density values using a Simpson's 1/3 rule integration. The mass-integral data was then tabulated as a cumulative distribution of mass-integral versus altitude. The source code for INTEG-_MI.BAS is listed in Appendix D. To increase accuracy and avoid round-off error, the mass-integral data was calculated in double precision to 16 significant digits. In hindsight, it would have been better to integrate the mass-integral from the maximum altitude downward in order to avoid round-off errors. At high altitudes, the difference between nearly equal mass-integral values requires extreme precision in the scale height values, since their difference is much less than 1. Integrating from the maximum altitude downward would involve the difference between two very different numbers because of the greater initial change in mass-integral with decreasing altitude. Significant round-off error could still be avoided even at low altitudes because of the much higher density relative to the higher altitudes, and hence the cumulative mass-integral would continue to change significantly. Also, since very few particles undergo transport

down to altitudes below about 20 kilometers, very few calculations would be required in these regions relative to higher altitude regions. Figure 2 shows a graphical representation of cumulative mass-integral as a function of geometric altitude.

The altitude regions defined for the density data were also used for the mass-integral data. An expression for the mass-integral as a function of geometric altitude was obtained by integrating equation (2) over each altitude region, and has the following mathematical form (for $z_i \leq z < z_{i+1}$)

$$MI(z) = MI(z_i) + \int_{z_i}^{z} \rho(z_i) \exp\left[-\frac{(z-z_i)}{S_i}\right] dz \qquad (5)$$

where

$MI(z)$ = mass-integral at specified altitude [g/cm^2]

$MI(z_i)$ = mass-integral at base altitude of i^{th} region [g/cm^2]

$\rho(z_i)$ = density at base altitude of i^{th} region [g/cm^3]

z = specified altitude [cm]

z_i = base altitude of i^{th} region [cm]

S_i = mass-integral scale height factor of i^{th} region [cm]

Performing the integration yields the following expression for the mass-integral as a function of geometric altitude

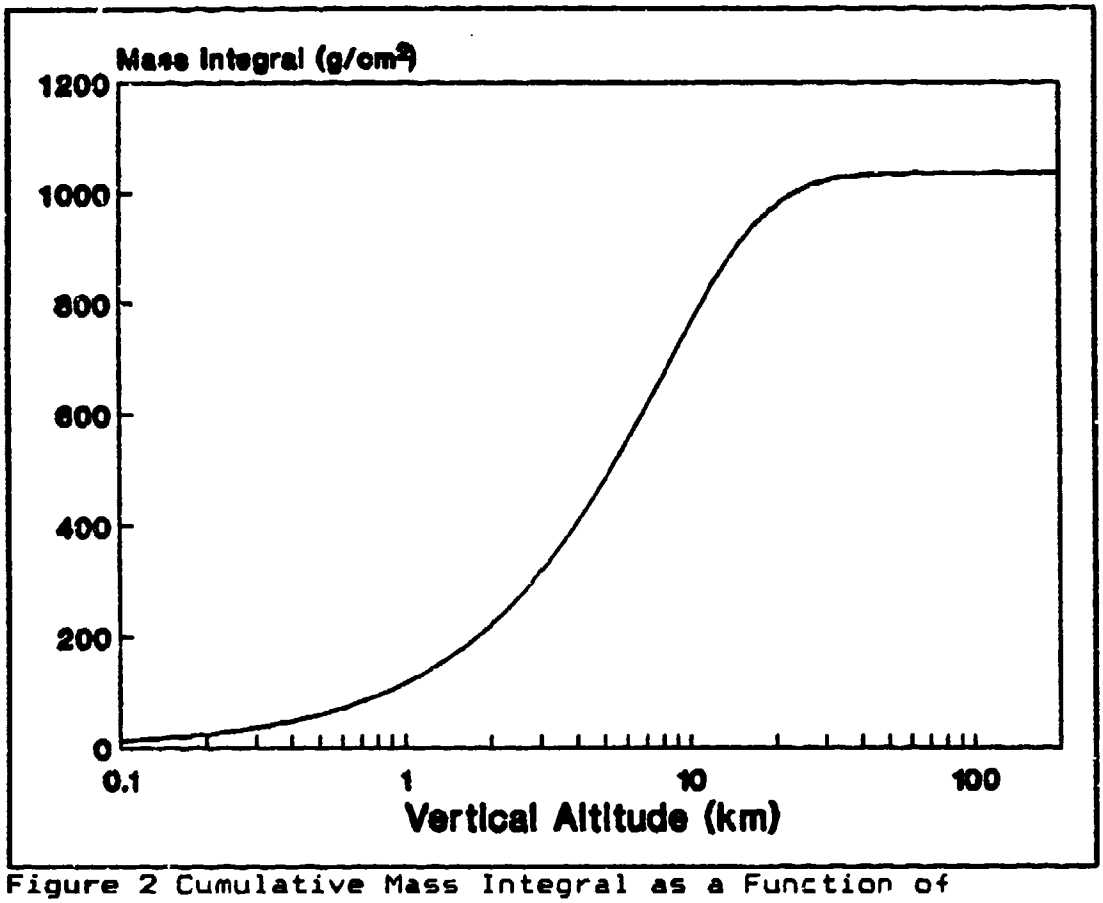

Figure 2 Cumulative Mass Integral as a Function of Geometric Altitude for a Polar angle of 0 Degrees

$$MI(z) = MI(z_1) + \rho(z_1) S_1 \left[1 - \exp\left(-\frac{(z - z_1)}{S_1}\right)\right] \qquad (6)$$

The parameters needed in equation (6) to calculate the mass-integral up to a maximum altitude of 990 km are presented in Table 3. Inverting equation (6) results in the following expression which calculates the altitude given a mass-integral

$$z = z_1 - S_1 \ln\left[1 + \frac{(MI(z_1) - MI(z))}{(\rho(z_1) S_1)}\right] \qquad (7)$$

The 36 atmospheric regions together with the corresponding parameters for mass-integral are listed in Table 3. The cumulative mass-integral at an altitude of 990 km, which represents the mass-integral at infinity, was found to be 1035.635131402448 g/cm². This value defines the upper limit of the atmospheric model, and was computed using equation (6).

Mass-Integral Scaling (MIS)

Describing radiation transport in detail involves using the Boltzmann transport equation. A full physics analytic treatment of the Boltzmann transport equation as it applies to radiation transport is rarely attempted. Because the density of air varies with altitude, numerical solution of the Boltzmann transport equation becomes prohibitive in terms of complexity and computational effort. As an alternative, radiation transport characteristics are studied through the use of Monte Carlo simulations. Monte Carlo techniques can provide excellent results by modelling the problem in two or three dimensions. Often, Monte Carlo simulations can provide results only for specific cases because of the high computational cost associated with this technique. This became the primary reason for developing faster computer programs which used the mass-integral scaling approximation.

Table 3: Atmospheric Parameters for Constant Mass-Integral Scale Height Regions

Region	Z_L [km]	Z_H [km]	MI [kg/m^3]	S_I [km^{-1}]
1	0	1	0.0000	10.3412402237278
2	1	2	116.76350000000	10.0998192414954
3	2	3	222.60716666667	9.8669317261947
4	3	4	318.33433333333	9.6450353272150
5	4	5	404.70453333334	9.4115591457853
6	5	10	482.43680000000	8.8809231258504
7	10	15	763.99446666667	6.928688443723
8	15	20	911.27230000000	6.374429797604
9	20	25	978.75926666667	6.261929959628
10	25	30	1009.3796200000	6.3973690617414
11	30	40	1023.2862866667	6.4755778050254
12	40	50	1032.6629466667	7.1036242751129
13	50	60	1034.8067933333	8.3821126459594
14	60	70	1035.4064800000	7.7650393215337
15	70	80	1035.5806097667	6.8327735117248
16	80	90	1035.6241078667	6.1260854547166
17	90	100	1035.6332051467	5.5727092615073
18	100	110	1035.6347923667	5.6886484922656
19	110	120	1035.6350561960	6.198139513 ,538
20	120	130	1035.6351043807	9.3510960917720
21	130	140	1035.6351180274	12.6721741503841
22	140	150	1035.6351236653	15.7852659297959
23	150	160	1035.6351265031	18.7015085627943
24	160	180	1035.6351281111	22.1902093305744
25	180	200	1035.6351297362	27.1428213479546
26	200	240	1035.6351304712	32.5722461137614
27	240	280	1035.6351310565	39.9158435804466
28	280	320	1035.6351312550	45.8484861083246
29	320	400	1035.6351313343	51.6265976153724
30	400	480	1035.6351313857	57.9144605754359
31	480	560	1035.6351313979	55.0126655594858
32	560	640	1035.6351314009	68.3636856102718

Table 3: (Continued)

Region	Z_L [km]	Z_H [km]	MI [kg/m^3]	S_L [km^{-1}]
33	640	720	1035.6351314019	78.3404006307542
34	720	800	1035.6351314022	98.1437260557627
35	800	880	1035.6351314023	139.178054965649
36	880	990	1035.6351314024	188.775256150840

Mass-integral scaling is a technique which involves approximating the fluence or dose in a variable density system with previously computed results of fluence or dose in a homogeneous system [2:2]. Discrete ordinates numerical solutions to the Boltzmann transport equation provide the computed results for an infinite homogeneous system. The computed results for the homogeneous system are then extended to a variable density system, i.e., the atmosphere. The scaling law which relates the mass-integrals in medium A with medium B, both with uniform density, is given by [2:2]

$$\rho_B r_B = \rho_A r_A \tag{8}$$

where

$\rho_B r_B$ = mass range at r_B in medium B

$\rho_A r_A$ = mass range at r_A in medium A

From equation (8), it follows that the $4\pi r^2$ fluence present at point A is also present at point B with the restriction that the density is uniform and the same isotropic point source exists in both systems. The scaling law above can be used to approximate the mass range in a homo-

geneous medium to the mass range in a variable density medium by [2:3]

$$MI = \rho_H r_H = \int_0^{r_v} \rho_v(r')\,dr' \tag{9}$$

where

$\rho_H r_H$ = mass-integral in a homogeneous medium

r_v = range in a variable density medium

$\rho_v(r')$ = position-dependent air density

MI = mass-integral

Figure 3 shows the coordinate geometry used in this analysis. Because of rotational symmetry, the azimuthal angle is not needed and is not shown. Since air density varies only with altitude, z, the mass-integral can now be defined by the following expression [2:3]

$$MI = \int_{z_s}^{z_d} \rho(z)\,\frac{dz}{(\sin\psi)} \tag{10}$$

where

z_s = altitude of the source

z_d = altitude of the detector (field point)

$\rho(z)$ = altitude-dependent air density

ψ = source elevation angle (see figure 3)

For small values of ψ, there is little change in altitude, and hence the density can be calculated based on a

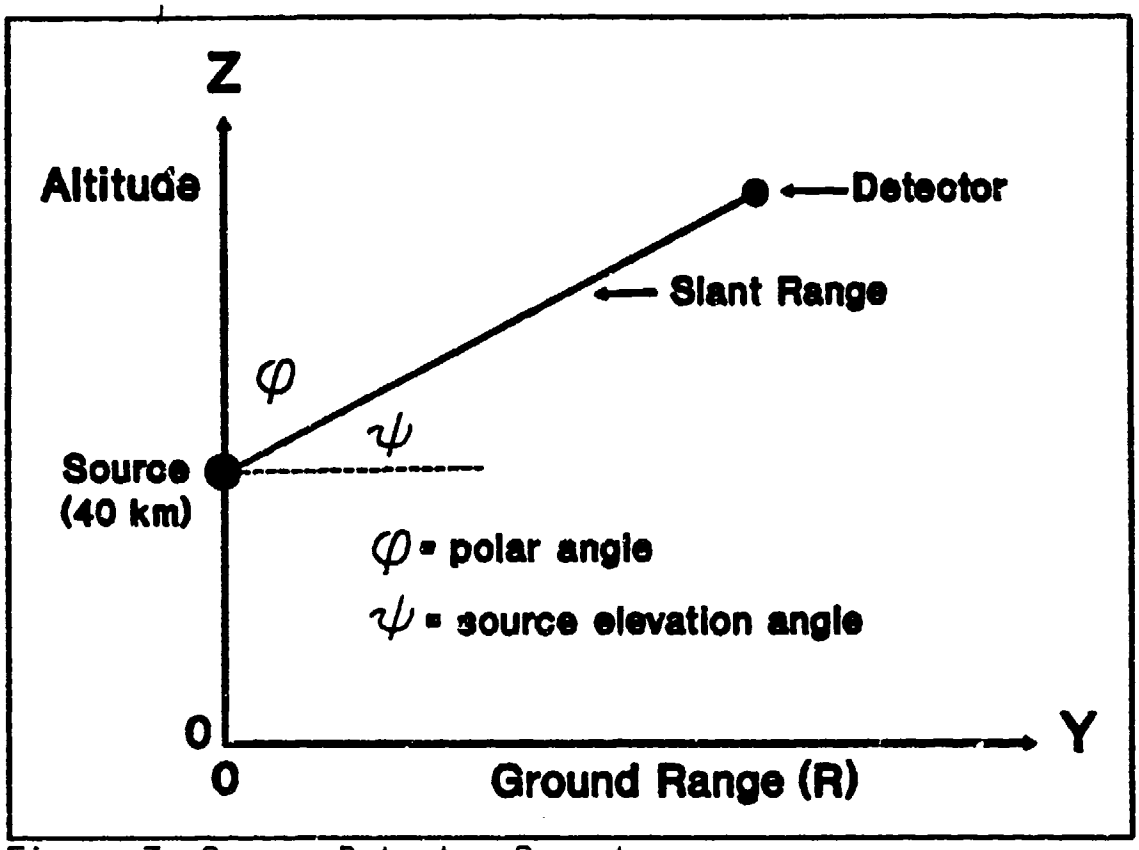

Figure 3 Source-Detector Geometry

simple average, $(z_s + z_d)/2$. Note that ψ represents the source elevation angle, and thus a correction for the mass-integral along a slanted path (see figure 3) has been incorporated into equation (10). For Monte Carlo calculations, the mass-integral as computed by equation (6) is for a vertical path only. A correction for a slanted path is found by dividing the difference in the mass-integrals at the two altitudes by the z-direction cosine, φ (see figure 3).

SMAUG-II uses results of $4\pi r^2$ fluence versus mass-integral based on a set of least-squares fits obtained from the computer code ANISN (ANIsotropic SN), a one-dimensional

discrete ordinates code. More details on SMAUG-II are provided in section III.

III. MCNP and SMAUG-II Code Descriptions

MCNP Code

MCNP [4:1] is a general-purpose, continuous-energy, generalized-geometry, time-dependent, coupled neutron-photon Monte Carlo transport code. MCNP is written in FORTRAN 77 and was originally developed by Los Alamos National Laboratory (LANL). It solves neutral particle transport problems and can be run in one of three modes: neutron transport only, photon transport only, or coupled neutron-photon transport, in which photons are produced through inelastic interactions of neutrons.

The user defines the problem parameters in a standard input file, INP, which is then read by MCNP. The input file contains information about the geometry, the source, the materials, the cross sections, and the tallies used. A sample input file used in this analysis is located in Appendix B. A complete discussion of Monte Carlo theory, use of MCNP, cross section libraries, and input cards is provided in the MCNP user's manual [4].

SMAUG-II Code

SMAUG-II [3; 2:4-5] is a computer program written in FORTRAN and was developed by the Air Force Weapons Laboratory. It computes the radiation effects from both neutron and gamma radiation from a neutron-photon point source within the atmosphere. Output results include free-field neutron

and photon fluences, energy fluences, mean energies, and absorbed tissue and silicon doses at field point locations specified by the user.

The source information was provided by the Air Force Weapons Laboratory and was furnished with the SMAUG-II program. The spectra included a 37-group neutron spectrum (in file TNS.NEV) and a 21-group photon spectrum (in file EXP.GAM). The default spectra used in SMAUG-II was also used in MCNP to facilitate comparisons. The neutron and photon spectra are given in Appendix F.

SMAUG-II employs mass-integral scaling based on discrete ordinates (SN) calculations of neutron and photon transport characteristics in an infinite homogeneous system. SMAUG-II uses a set of 1711 empirical transmission functions that are least-squares fits to neutron and photon transport results calculated with the computer code ANISN (ANIsotropic SN). ANISN is a one-dimensional discrete ordinates code for performing transport calculations in a homogeneous medium. ANISN uses the DLC-31 multigroup cross section set provided by Oak Ridge National Laboratory (ORNL) for these calculations. ANISN also uses an air density of 1.11 mg/cm^3 and an atmospheric composition of 79 percent nitrogen and 21 percent oxygen.

Additional information concerning SMAUG-II can be found in AFIT Technical Report AFIT/EN-TR-90-5 [2:4-5]. Details on using SMAUG-II can be found in the SMAUG-II user's guide [3].

A sample SMAUG-II input/output file listing used in this analysis is provided in Appendix C.

IV. MCNP Modifications

Once the parameters for the atmospheric model were determined, modifications of MCNP began. This section will present information on MCNP program flow and an overview concerning calculations used in the user-written subroutines and functions. Topics discussed include: Program flow of Subroutines HSTORY and TRANSM, where most of the particle transport takes place, reference density, calculation of two main transport parameters, and the required auxiliary modifications to MCNP. For additional information on MCNP program flow, see the MCNP user's manual [4:38-40]. Additional specific information concerning the MCNP modifications is given as an addendum to this thesis [7], where copies of all the affected MCNP subroutines, user-written subroutines and functions can be found.

Transport Program Flow

Particle transport in MCNP is controlled via the main transport overlay MCRUN. MCRUN calls subroutine TRNSPT to start particle histories via subroutine HSTORY.

Subroutine HSTORY. Subroutine HSTORY begins the particle history by starting a particle from the source via subroutine STARTP. All source parameters such as initial direction, weight, and energy are determined. Initial source parameters are next checked against user-supplied weight cut-offs and energy cut-offs and some summary information is

incremented. Subroutine TALLY is called to score tally contributions during a particle history. If point detectors or ring detectors are being used, then subroutine TALLYD is called from TALLY to score contributions to detectors. If DXTRAN spheres are being used, then DXTRAN is called to score DXTRAN sphere contributions. The weight window variance reduction game is played if requested, and energy splitting or Russian roulette is performed if required.

Back in subroutine HSTORY, particle transport continues by calling TRACK to determine the intersection of the particle trajectory with each bounding surface of the cell. The distances to the nearest cell boundary, DLS, time cut-off, DTC, and DXTRAN sphere, DXL, are calculated. Cross sections for the cell are determined via subroutines ACETOT for neutrons and PHOTOT for photons. A macroscopic cross section, QPL, is calculated and then modified by the exponential transform in subroutine EXTRAN, if necessary. The distance to next collision, PMF, is determined by a random number sampling of a logarithmic distribution. Up to this point, no modifications were made to subroutine HSTORY.

The track length in the cell is determined by taking the minimum of the distance to collision, PMF, the distance to time cut-off, DTC, the distance to the nearest bounding surface, DLS, and the distance to a DXTRAN sphere, DXL. The particle will undergo a collision only if the distance to collision, PMF, is less than the distance to a surface cros-

sing, DLS. Subroutine TALLY is called to increment any cell tallies if necessary and some summary information is incremented. The particle's position is also updated. The energies and directions of the particles exiting a collision site are handled in subroutines ACECAS and ACEOS.

Subroutine TRANSM. Subroutine TRANSM is called from TALLYD to calculate the total transmission to the detector. Prior to calculating the transmission, subroutine DDDET is called to calculate the distance, DD, to the detector and TRACK is called to calculate the distance to the nearest intersecting surface, DLS.

Cross sections for the cell are determined via subroutines ACETOT for neutrons and PHOTOT for photons. Once the microscopic cross section in the cell has been determined, it is multiplied by the atom density in the cell to obtain the macroscopic cross section. The track length in the cell, D, is determined by taking the minimum of the distance to the nearest bounding surface, DLS, and the distance to the detector, DD. The number of mean free paths to the detector or nearest bounding surface, AMFP, is determined using the values of the macroscopic cross section in the cell, PLE, and the minimum distance to the detector or nearest bounding surface, D. Then the locations of the new cell and particle position are updated.

Reference Density

Modelling the variable density atmosphere involved

defining a reference air density. In the unmodified version, MCNP computes density-dependent parameters using a discrete cell density defined in the input file. In the modified version, the variation of air density is continuous, and a constant density spatial mesh in the vertical direction is no longer needed; cells are needed only for splitting/Russian roulette. Therefore, in the modified version of MCNP, the air density in each cell is redefined to be the mass density at sea-level, 1.225×10^{-3} g/cm^3, regardless of the values read from the input file. All subsequent calculations of density-dependent parameters will now be calculated based on a sea-level homogeneous atmosphere. At this point, prior to computing the distance to collision or the transmission to the detector, the MCNP calculations are intercepted. The aforementioned parameters are then corrected for a variable density atmosphere.

Prior to running the MCRUN overlay, the main overlay IMCN is run to read the input file to obtain the necessary parameters used in defining the problem. Subroutine NEXTIT is called to process items from the input file, i.e., to store such parameters as material density and cell descriptions. Subroutine NEXTIT was modified for the purpose of redefining the density in each cell to be the density at sea-level.

Transport Parameters

In Monte Carlo transport calculations, there are two

principle parameters that involve determining the optical path length between two points in space: 1) the sampled distance to collision and 2) the number of mean free paths to a detector or nearest intersecting boundary. Both parameters are closely related and depend strongly on the atmospheric density. Details of the calculation of each of these two important transport parameters is presented below.

Distance To Collision. The distance to collision, PMF, computed in HSTORY, is based on the microscopic cross section in the cell and the atom density in the cell, which was redefined in NEXTIT to be the air density at sea-level. This is given by

$$PLE = TOTM * DEN(CELL) \qquad (11)$$

where

PLE = macroscopic cross section in current cell [cm^{-1}]

TOTM = microscopic cross section in current cell for either a neutron or photon reaction [barns/atom]

DEN(CELL) = atom density in current cell [atoms/barn-cm]

Since the distance to collision is a probability based on density, it is necessary to correct this value for a variable density atmosphere. Subroutine EQDIST, called from HSTORY, was written to calculate the corrected distance to collision based on values input from HSTORY, i.e., current particle altitude, z-direction cosine, and distance to collision based on a sea-level homogeneous atmosphere. Calculation of the

required quantities used to determine the corrected distance to collision are explained below. See figure 3 for the general coordinate geometry used in this analysis. The variable names referenced in the discussion below are the variable names used in the non-MCNP (user-supplied) subroutines or functions.

The unmodified version of MCNP computes distances in units of distance, centimeters. However, the variable density atmospheric model computes distances in units of mass range, g/cm^2. Therefore, before correction for a variable density atmosphere can be made, it was first necessary to transform the MCNP-computed distance to collision, PMF (EDST in subroutine EQDIST), from units of centimeters to an equivalent mass range in units of g/cm^2 for a sea-level homogeneous atmosphere. This equivalent distance was then corrected for a variable density atmosphere using the MCNP modifications.

The mass-integral along the particle path in a homogeneous sea-level atmosphere is calculated using the following equation

$$MIPDH = 1.225 \times 10^{(-3)} EDIST \qquad (12)$$

where

MIPDH = equivalent mass range along particle path in a sea-level homogeneous atmosphere [g/cm^2]

EDIST = distance to collision in a sea-level homogeneous

atmosphere [cm]

This calculation is performed in function DMI.

The cumulative mass-integral, MICA, at the current particle altitude, ZO, can be computed using equation (13) below once the scale height region has been determined. For $(z_i \leq zO \leq z_{i+1})$

$$MICA = MI(z_i) + \rho(z_i) S_i \left[1 - \exp\left(-\frac{(zO - z_i)}{S_i}\right)\right] \qquad (13)$$

where

MICA = mass-integral at current particle altitude [g/cm^2]

$MI(z_i)$ = mass-integral at base altitude of i^{th} region [g/cm^2]

$\rho(z_i)$ = density at base altitude of i^{th} region [g/cm^3]

zO = current particle altitude [cm]

z_i = base altitude of i^{th} region [cm]

S_i = mass-integral scale height factor of i^{th} region [cm]

This calculation is performed in function MASI.

Though the collision altitude, ZC, is still unknown, the values of MIPDH, MICA, and the z-direction cosine, WO, can be used to determine the required cumulative mass-integral, MICP, at the collision altitude, ZC. MICP is computed based on the known mass range to collision, MIPDH. This calculation is performed by calling function MIZ.

$$MICP = MICA + MIPDH * W0 \qquad (14)$$

where

MICP = required mass-integral at collision altitude [g/cm^2]

MICA = mass-integral at current particle altitude [g/cm^2]

MIPDH = mass-integral along particle path to collision in a sea-level homogeneous atmosphere [g/cm^2]

W0 = z-direction cosine

At this point, a check is made to compare the computed cumulative mass-integral at the collision altitude, MICP, with the mass-integral at infinity, MIINF, defined to be 1035.635131402448 g/cm^2, the cumulative mass-integral at the 990 km altitude limit. If MICP is greater than MIINF, then Subroutine EQDIST is exited and PMF is set to HUGE, a very large number used by MCNP, effectively eliminating any collisions along the current particle track. If MICP is less than or equal to MIINF, then the collision altitude, ZC, is determined using the following expression

$$zc = z_1 - S_1 \ln\left[1 + \frac{(MI(z_1) - MI(zc))}{(\rho(z_1) S_1)}\right] \qquad (15)$$

For cases where the z-direction cosine, W0, becomes very small (nearly co-altitude relative to the current particle position), the change in density is very small along the

particle path. Therefore, the average density between the current altitude and the collision altitude is used. In this case, the difference between the current altitude and collision altitude is ≤ 10 meters. The air densities are calculated by calling function DNTY.

Finally, the distance to collision, PMF (EDST in Subroutine EQDIST), corrected for a variable density atmosphere, can be computed by calling function EQUIVDST. Function EQUIVDST accepts as inputs the collision altitude, ZC, the current particle altitude, ZO, the z-direction cosine, WO, the mass-integral along the particle direction in a homogeneous sea-level atmosphere, MIPDH, and the densities (calculated only if WO is small). For cases where WO is not small, the corrected distance to collision is given by

$$EDST = \frac{(ZC - ZO)}{WO} \tag{16}$$

where

EDST = distance to collision corrected for a variable density atmosphere [cm]

For cases where WO is small, the density is nearly constant along the partirle path, hence the corrected distance to collision is given by

$$EDST = \frac{MIPDH}{[(DENCA + DENCP)/2]} \tag{17}$$

where

DENCA = air density at current particle altitude [g/cm^3]

DENCP = air density at collision altitude [g/cm^3]

Mean Free Paths To Detector or Boundary. Contributions to a detector are made at every source or collision point by creating and transporting a pseudoparticle directly to the detector. The total transmission to the detector depends on several factors: 1) the exponential attenuation through the medium, 2) a probability density function for scatter toward the detector, 3) spherical divergence, which accounts for the solid angle effect, and 4) the particle weight.

The only one of the aforementioned parameters that depends on atmospheric density is the exponential attenuation term. The attenuation term represents the total attenuation of the radiation by the atmosphere along the particle path over a given number of mean free paths. The attenuation along the particle path to a detector is given by the following relation

$$A=\exp(-AMFP) \qquad (18)$$

where

A = attenuation along the particle path

AMFP = number of mean free paths to the detector or nearest intersecting boundary

At this point, MCNP computes the distance to the detector, DD, using subroutine DDDET. MCNP next determines

the minimum of the distances to the detector or the nearest intersecting boundary. MCNP now computes the macroscopic cross section in the cell, PLE, for a sea-level homogeneous atmosphere using equation (11). It is necessary to correct the macroscopic cross section in the cell, PLE, for a variable density atmosphere using subroutine EQDIST. A flag is set prior to calling EQDIST in subroutine TRANSM to indicate the origin of the calling statement, either subroutine HSTORY or subroutine TRANSM. The value of the flag, either 0 or 1, will determine the specific calculations that are performed.

Prior to calling EQDIST, the reciprocal of the macroscopic cross section, XMFP = 1/PLE, is computed to give the mean free path in a sea-level homogeneous atmosphere (recall that MCNP first calculates all density-dependent parameters based on sea-level density in each cell). EQDIST is then called from subroutine TRANSM with the mean free path, XMFP, the current altitude, ZZZ, the z-direction cosine, WWW, the calculation flag, NINP, and the track length in the cell, D, as inputs.

In subroutine EQDIST, it is first necessary to transform the MCNP-computed minimum distance to the detector or nearest intersecting boundary, D, from units of centimeters to an equivalent mass range in units of g/cm^2 in a sea-level homogeneous atmosphere. This equivalent mass range is then used to correct the macroscopic cross section, PLE, for a variable

density atmosphere.

In subroutine EGDIST, the altitude of the detector or nearest intersecting bounding surface is determined using the following equation

$$ZD=Z0+W0*DTD \qquad (19)$$

where

ZD = altitude of detector or intersecting boundary [cm]

Z0 = current particle altitude [cm]

W0 = z-direction cosine

DTD = distance to detector or intersecting boundary [cm]

The mass-integral along the particle path in a homogeneous atmosphere, MIPDH, is next calculated using equation (12). Function DMI performs this calculation.

Next, the cumulative mass-integral at the current particle altitude, MICA, and the cumulative mass-integral at the detector or intersecting boundary altitude, MIDA, is computed using equation (6). This calculation is performed in function MASI.

The mass-integral along the particle path in a variable density atmosphere, MIPD, can now be determined using the following relation (for W0 not too small)

$$MIPD=\frac{(MIDA-MICA)}{W0} \qquad (20)$$

where

MIPD = mass-integral along the particle path in a variable density atmosphere [g/cm^2]

For cases where the z-direction cosine, WO, becomes very small (nearly co-altitude relative to the current particle position), the average density between the current altitude and the collision altitude is used. In this case, the difference between the current altitude and collision altitude is $\leq$ 10 meters. The air densities are calculated by calling function DNTY. For small values of the z-direction cosine, WO, MIPD is computed using the following relation

$$MIPD = DTD * \left[\frac{(DENCA + DENCP)}{2} \right] \qquad (21)$$

where

DTD = minimum distance to the detector or nearest intersecting boundary [cm]

DENCA = air density at current particle altitude [g/cm^3]

DENCP = air density at collision altitude [g/cm^3]

Recall that the minimum of the distances to the detector and nearest intersecting boundary, D, was first transformed into an equivalent mass range, MIPDH. The corrected mass range in a variable density atmosphere, MIPD, was then computed. It is now possible to correct the mean free path to the detector or nearest intersecting boundary, EDST, for a variable density atmosphere. This can be calculated using

$$EDST = \frac{(EDST * MIPDH)}{MIPD} \qquad (22)$$

where

EDST [LHS] = corrected mean free path [cm]

EDST [RHS] = uncorrected mean free path [cm]

MIPDH = mass integral along particle path in a sea-level homogeneous atmosphere [g/cm^2]

MIPD = mass integral along particle path in a variable density atmosphere [g/cm^2]

Back in TRANSM, the corrected macroscopic cross section in the cell, PLE, is found by taking the reciprocal of the corrected mean free path, EDST (defined as XMFP in MCNP), where EDST is given by equation (22). Finally, the cumulative total number of mean free paths to the detector or nearest boundary over all cells traversed by the particle trajectory, is found from the following equation

$$AMFP = AMFP + PLE * D \qquad (23)$$

where

AMFP [LHS] = cumulative total number of mean free paths to the detector or nearest boundary along the particle path

AMFP [RHS] = number of mean free paths along the particle path in the current cell

AMFP here is equal to PLE*D.

Auxiliary Modifications

The auxilliary changes necessary to complete the MCNP modifications are explained in this section. Details of each of the affected subroutines not mentioned above will be provided to complete the modification package.

Data Block ATINIT. A user-defined data block which initializes the arrays containing parameters which define the variable density atmospheric model. The arrays are stored in a user-defined common block /ATCOM/. Common block /ATCOM/ is defined in the file CM.inc.

Subroutine IMCN. As mentioned above, this subroutine is the main overlay subroutine, and controls the input and sorting of the problem data.

Modifications: 1) Comment printed to the terminal informing the user that the variable density version of MCNP was being run.

Comdeck CM.inc. This include file serves as the main common block declaration file for all overlays used in MCNP.

Modifications: 1) Common block /ATCOM/ defined and contains the necessary arrays that store the various parameters defining the atmospheric density model.

Comdeck ZC.inc. This include file serves as an auxiliary comdeck file to comdeck CM and defines processor-dependent constants and parameters and also dimensions general constants and I/O unit numbers.

Modifications: 1) Two message lines defined to inform

user of MCNP version and for error statement in subroutine EQDIST. 2) Dimension variables defining the number of atmospheric regions and number of scale height factors.

Subroutine NEXTIT. This subroutine controls the processing of input items.

Modifications: 1) Density for all cells redefined to be 1.225×10^{-3} g/cm^3, the mass density of air at sea-level, regardless of input value.

There are absolutely no changes required for the standard input file, INP. Cell density values defined in the input file are required, but specific values are irrelevant, as they will be redefined within MCNP, and thus have no effect on results.

V. MCNP INPUT PARAMETERS

This section describes the various input parameters used in defining the problem. The discussion includes practical details on the geometry, the source spectra, the material specifications, the variance reduction techniques, the cross sections, and the tallies used. The above parameters are defined in the MCNP generic input file, INP. A sample input file used in this analysis is given in Appendix B. The neutron and photon source spectra are given in Appendix F.

Problem Geometry

The primary goal in determining the geometry for a particular problem is to model, as accurately as possible, the geometric features and the material properties that are inherent in the problem definition. A secondary goal is to obtain the simplest geometry possible without overly compromising its validity. By retaining certain symmetries in the problem, the complexity and computational effort can be reduced.

The only geometric feature inherent in the atmosphere is the airspace itself. The inherent material feature in the atmosphere is the variation of air density with changing altitude. Density values vary several orders of magnitude over a few tens of kilometers, which can drastically affect the transport characteristics of the radiation. The goal, therefore, is to develop a suitable geometry which "contains" the surrounding airspace within certain geometrical limits

while utilizing the variable density atmospheric model.

Cylindrical (r,z) geometry is appropriate because of the variation of air density in only the vertical (or z) direction and the inherent azimuthal or "rotational" symmetry about the z-axis. To take advantage of this symmetry, cylinders of various radii were used to define the vertical surfaces, while planes at various altitudes were used to define the horizontal surfaces. A graphical representation of the geometry used in determining the neutron and photon fluences at ranges at the source altitude of 40 kilometers is shown in figure 4.

As seen in figure 4, only the right half of the cylinder is shown, due to the z-axis symmetry. The problem has been modelled in three dimensions with the restriction that rotational symmetry be employed. The geometry has been divided up into discrete partitions or cells. Each cell is defined separately in the input file and referenced by a user-defined cell number. Each cell is defined by referring to surfaces which bound the cell by a surface number. In this case, surface numbering begins with the innermost cylinder (surface 1), progresses outward until the outermost cylinder is reached (surface 23), and then begins at ground level (surface 24) and continues upward until the top-most surface is reached (surface 27). Detailed information on the basic concepts of MCNP geometry can be found in the MCNP user's manual, Chapter 1, section III [4:12-19].

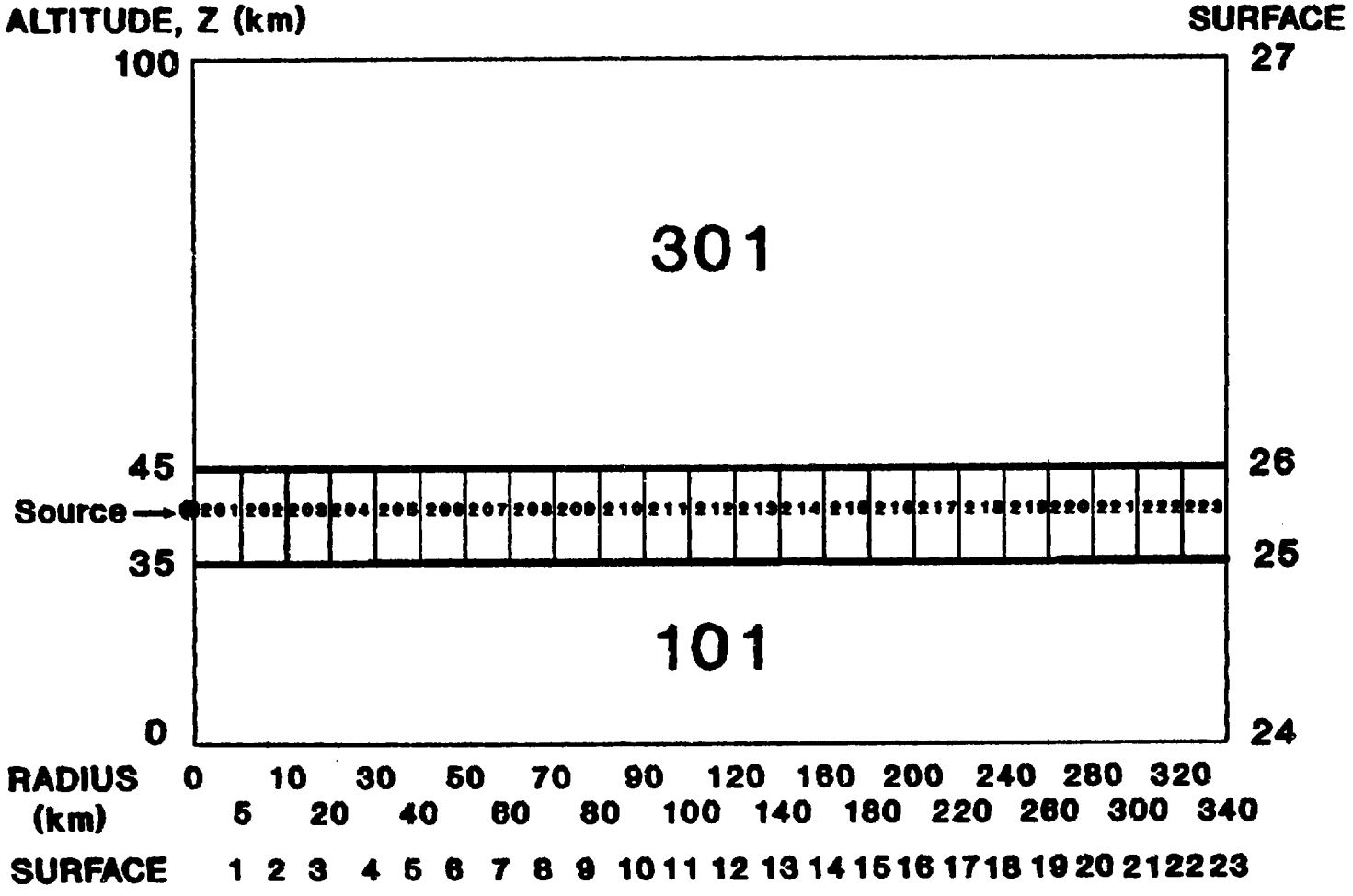

Figure 4 Spatial Cell Geometry for Co-Altitude Detectors

The cell structure shown in figure 4 was chosen to provide adequate particle splitting/Russian roulette (see variance reduction below) along source co-altitude ranges out to a maximum detector range of 250 km. Variance reduction is not needed outside this co-altitude region. Since the Monte Carlo code MCNP was modified to provide a continuously varying atmospheric density with altitude, constant density spatial cells are no longer needed in the vertical direction to represent the variation of air density. Thus, the atmospheric regions outside the co-altitude region can be represented with just two cells. This extra airspace is needed for those particles that possess a finite probability of contributing to the final result by scattering either upward or downward and then reflecting towards the point of interest. There are only 25 cells needed in the co-altitude case (see figure 4) as compared to 181 cells required for the same type of study in previous work. This considerably simplifies the problem geometry and saves computational effort. Cell geometry was appropriately modified for other source-detector scenarios.

Source Spectra

There were two source spectra provided with the SMAUG-II code [4]. The spectra included 37 neutron energy groups ranging from thermal energies to a maximum of 14.2 MeV and 21 photon groups ranging from 10^{-2} MeV to a maximum of 14 MeV. The neutron and photon spectrum energies and corresponding

energy bin probabilities are listed in Appendix F. The default spectra provided with the SMAUG-II code were used in MCNP to facilitate the comparisons between SMAUG-II and MCNP. The source spectra were not classified, but rather generic, unclassified spectra provided with the computer code SMAUG-II.

During the course of the Monte Carlo simulations, an attempt was made to provide for both source neutrons and source photons in the same MCNP run. As a consequence, secondary photon results could have been obtained. To accomplish this, it would have been necessary to generate source neutrons (via a neutron source spectrum) and primary source photons (via a photon source spectrum) within the same MCNP run. These attempts were unsuccessful, and it is unknown if generating multiple particles from multiple source spectra is possible within MCNP. As a result, each MCNP simulation was repeated twice, once using the neutron spectrum and once using the photon spectrum. To obtain the total photon free-field fluence at a point of interest, the secondary photon fluence obtained based on the neutron source spectrum and the primary photon fluence obtained based on the photon source spectrum would be summed.

The source spectra energy bin probabilities were provided with SMAUG-II, and were also used in the MCNP input file. The energy bin probabilities were normalized to one. See Appendix B for an example of a neutron source spectrum

definition. The units for the spectra are: "neutrons per MeV per source neutron" for the neutron spectrum and "photons per MeV per source photon" for the photon spectrum.

Material Specifications

The primary constituents of the atmosphere are nitrogen, oxygen, and argon, in order of abundance. These elements normally make up about 99.9 percent of the earth's atmosphere. The remaining trace constituents, which make up the remaining 0.1 percent of the atmosphere, represent negligible neutron and photon absorption and scatter cross sections, and thus were not included in this analysis. Specific material specifications can be found in the sample input file, Appendix B.

Variance Reduction

The flexibility of MCNP enables the code to provide a wide variety of variance reduction techniques to aid the user in obtaining peak efficiency for a particular problem. In addition to the information provided in MCNP [4:122-148], the Los Alamos report "A Sample Problem for Variance Reduction in MCNP" [6] provides useful information concerning the application of variance reduction schemes offered by MCNP. The only variance reduction technique employed in this analysis was geometric splitting/Russian roulette, and is discussed briefly below.

Geometric Splitting/Russian Roulette. This is the most

widely used variance reduction technique in Monte Carlo analysis. This technique is the most effective first step in obtaining substantial gains in efficiency. Geometric splitting/Russian roulette was employed in this analysis to aid in particle penetration over long distances (large mass ranges). At low altitudes, (ground level to several tens of kilometers), the air density is such that the mean free path of neutrons is on the order of several hundred meters. If the point of interest is several tens of kilometers distant, then this represents an optically thick problem, and a large amount of particle splitting is needed. Less splitting is needed at the higher altitudes because of decreasing air density.

In order to transport these particles over long distances, splitting surfaces (defined in the problem geometry) are required. Geometric splitting/Russian roulette is only needed in the general direction of the detector locations. The ultimate goal is to uniformly sample the track-length estimate of the cell flux by maintaining an even particle population in each cell along the direction to the detector. Additional details concerning this procedure can be found in the Los Alamos report LA-10363-MS [6:7] or AFIT Technical Report AFIT/EN-TR-90-5 [2:15].

Cross-Sections

The primary evaluated source of cross section data for MCNP has been the ENDF/B system. Specific details regarding

data tables included with MCNP (version 3B) and their formats are contained in the MCNP manual [4:485].

Several classes of nuclear data tables are included with MCNP. The principle nuclear and atomic interaction data classes (there are 5 total) include: 1) continuous-energy, 2) discrete energy, and 3) multigroup. Details on each of these data classes is provided in the MCNP manual. For this analysis, continuous-energy data tables were used throughout the analysis in order to extract the most accurate cross section information from the given data. For the exact table used, see the sample input file, under material parameters, in Appendix B. A brief discussion of continuous-energy data tables is provided below.

Continuous-energy data tables contain cross sections for each type of reaction, given over an energy grid sufficiently dense that linear interpolation between the data points results in an interpolation error of normally not more than one percent. Angular distributions, photon interaction data, and secondary photon production data are included with this type of data table. Use of continuous energy data tables will usually increase run time and will require a larger amount of computer memory [4:48]. The specific cross section library used in the MCNP simulations was the BMCCS library set taken from ENDF/B-IV. Specific details for this library set can be found in the MCNP user's manual [4:523-557].

Tallies

MCNP provides a wide variety of tallies and detectors, six types for neutrons and five types for photons. Each tally or detector result is normalized to one source particle. Descriptions for these tallies are provided in the MCNP manual [4:80-82]. For this analysis, only ring detectors were used. For details on ring detector specifications, see the MCNP user's manual [4:219-246]. A brief discussion on ring detectors and the reasons for using them is given below.

A point detector is known as a "next event estimator" because it is a tally of the flux at a point if the next event is a trajectory without further collision directly to a point detector [4:88]. Contributions to a detector are made at every source or collision point by creating and transporting a pseudoparticle directly to the detector.

A ring detector tally is a point detector tally where the point detector tally is sampled at a location along a ring. A ring detector is useful when there is at least one degree of symmetry about a coordinate axis, in this case, the z-axis. Ring detectors were the ideal choice for obtaining time-independent flux (fluence) results for both neutrons and photons because they enhanced the efficiency of results over those obtained with point detectors.

Because the use of point detectors or ring detectors involves the creation and transport of psuedoparticles, they

are computationally expensive. However, ring detectors become useful and even necessary when there are few scattering events near the detector location. In these cases, the use of cell or surface tallies is often impossible. Also, when cells become very large, computing a cell average tally becomes meaningless, and thus ring detectors are ideal.

VI. Results and Discussion

Introduction

In section IV, the implementation of the MCNP modifications for a variable density atmosphere was discussed. This section will present topics that include validation of MCNP modifications and neutron-photon fluence results obtained with MCNP and SMAUG-II.

Validation of MCNP Modifications

Testing of the MCNP modifications was accomplished in two phases: 1) each subroutine or function using one of the fitting equations, either density or mass integral, was tested and 2) then the modified MCNP code was tested as an integrated whole. Each phase of the validation study is presented in turn below.

Phase 1. Each new function or subroutine was individually tested using a personal computer and Microsoft Fortran 4.1 to ensure calculational accuracy. Each scale height factor was computed using TK Solver to 16 digit precision. This was essential for two reasons. First, because MCNP calculates variables in cgs units, the scale height factors became quite large (units of cm^{-1}). Slight truncation in the scale height factor caused substantial errors in the computed density or mass-integral data. Second, the cumulative mass-integral data was computed from ground level upward to infinity. Therefore, substantial errors resulted in the

computed values of the scale height factors because often two nearly equal mass-integral values, especially at high altitudes, were involved in the calculations.

Before any of the subroutines were written, it was first necessary to verify both the accuracy of the scale height factors computed with TK Solver and the accuracy of the fitting functions. The primary goal in performing the testing was to ensure that the computed values of air density closely approximated the reference values taken from the U.S. Standard Atmosphere Tables, 1976.

For the density and mass-integral fitting functions, equations (2), (3), (6) and (7) together with TK Solver were used to verify both the density and mass-integral scale height factors for each scale height region. The density scale height factors were verified by choosing reference density values at each scale height region and inserting them into equations (2) and (3). Once the reference density at the base altitude and the altitude of interest were inserted, the computed value of the scale height factor could be verified by using the built in iterative solver supplied with TK Solver.

After the scale height factors for density were verified, it was necessary to calculate the relative accuracy of the computed density values. Using 36 scale height regions resulted in relative differences, found by comparing calculated density values to reference density values, that were

less than 0.1 percent in all but two or three of the upper altitude regions. The maximum relative difference was found to be less than 1 percent over all altitude ranges. In the upper altitude regions, the size of the scale height regions increased, leading to larger and less accurate scale height factors. These upper atmospheric regions were not subdivided into smaller regions in order to decrease the computer overhead associated with the array searches and because the upper atmospheric regions are far less important than the intermediate altitudes which are near the source altitude.

The cumulative mass-integral data was computed by integrating a table of reference density values using a Simpson's 1/3 Rule numerical integration algorithm written by the author (see Section IV, "Computing the Integrated Mass-Density"). Simpson's 1/3 Rule method has a global error of $O(h^4)$, where h is the vertical panel width for the altitude data. The errors associated with such a high order numerical integration routine are small, and on the order of the relative errors associated with the density results. The mass-integral scale height factors were verified in much the same way as the density scale height factors. In this case, mass-integral values were chosen at random for each scale height region instead of reference density values.

Past studies performed by Culp et al. relied on a constant density spatial mesh using a single 7 kilometer scale height factor to represent the variation of air density

with altitude. The errors introduced in representing the density variation in this way could be substantial, ranging from just a few percent for narrow altitude regions to 50 percent or more for wide altitude regions. Narrowing the altitude regions increased the relative accuracy of the density variation, but at a cost of increased run time due to the increase in the number of cells needed in defining the problem.

Several iterations were required to determine the proper number of scale height regions (36) in order to obtain the lowest possible relative error ($\leq$ 1 percent). The scale height factors for both density and mass-integral were recalculated each time the boundaries of the scale height regions were changed.

To fully model the density variation in the atmosphere, subroutines and functions were written which were later implemented as auxiliary modules in the MCNP code. These subroutines and functions are explained in Section IV. The parameters for the variable density exponential atmosphere, which included the altitudes, the density values, the computed mass integral values, and the scale height factors, were loaded into data arrays as table look-up values. Each subroutine or function module was tested separately using a personal computer and Microsoft Fortran 4.1 to ensure calculational accuracy. Calculations for both the density and mass-integral equations presented in Section IV were first

performed by hand. Calculations were then verified by computer before incorporating them into a particular subroutine. Next, each subroutine was individually tested for calculational accuracy.

Phase 2. Once all the subroutines had been verified for proper operation, they were incorporated into the MCNP code and then tested. A two-part approach was used to validate the accuracy of the modified MCNP code results: 1) run a Monte Carlo simulation from a past study (Culp et al.) and 2) run a series of simpler MCNP simulations using a scaled-down geometry.

Phase 2, Part 1. The study chosen was an investigation of neutron fluences using ring detectors at surfaces of constant range versus selected source elevation angles [2:29]. A maximum detector range of 50 kilometers was imposed because of the number of cells required when running the unmodified MCNP code. Fluence results from the previous study were compared to those obtained with the modified MCNP code. The comparison showed a relative difference of approximately 2 percent. As a first step, this comparison demonstrated that the results obtained with the modified MCNP code were reliable.

Phase 2, Part 2. As a next step in the validation, simpler simulation studies using the unmodified MCNP code were performed. These studies were accomplished with scaled-down geometries. Fine-mesh spatial grids with accurate

average densities in each scale height region were incorporated into the input files. The average densities in each region were computed using the newly-developed atmospheric density model to give the most accurate comparison. The simulations involved small geometries using cylinders of a few tens of kilometers in radius and height. The atmospheric region was centered around the primary source altitude of 40 kilometers. Again, fluence results using both ring detectors and cell tallies from the unmodified MCNP code were compared with those obtained with the newly-modified MCNP code. The comparison showed a relative difference of approximately 1 percent. A closer comparison was reasonable since the density variation as modelled using a spatial grid more closely approximated a continuously varying density. Several validation simulations of this type were run, using ring detectors and cell tallies at varying locations out to a maximum range of 50 kilometers. The maximum relative difference between the unmodified and modified MCNP codes was found to be not more than 1 percent. This also demonstrated that the modified MCNP was functioning properly.

To increase confidence in the proper functioning of the modified MCNP code, comparisons were made of the diagnostic information printed in the MCNP output file. The diagnostic information was compared to see if hidden bugs could be found. Important parameters for comparison were: 1) particle tracks escaping, number-weighted energy, flux-weighted

energy, and detector diagnostic information such as detector transmissions. For details on interpreting MCNP output, see the MCNP user's manual [4:312-413].

MCNP and SMAUG-II Results

MCNP neutron and photon fluence results are listed in Appendix A together with corresponding error estimates. The SMAUG neutron and photon results are also listed in Appendix A. Only the most representative MCNP and SMAUG-II data have been presented here. Appendix A contains numerous other MCNP and SMAUG-II results for other altitude-range combinations.

Neutron Fluence at 40 km. Figure 5 shows a comparison between MCNP and SMAUG neutron fluence results at an elevation of 40 kilometers (source altitude) versus radius (slant range in this case). Figure 6 shows the same results versus mass-integral. The MCNP results were computed using ring detectors and all results are normalized to one source particle. For comparison purposes, a line showing spherical divergence for one source particle has been plotted.

Close to the source (0-3 kilometers), the neutrons exhibit a streaming (spherical divergence) behavior. At 3 kilometers, the mass range is not more than 1.2 g/cm^2, as seen in figure 6. At intermediate radii (3-60 kilometers), buildup from neutron scattering contributions dominates over attenuation along the source co-altitude band. This results in a higher neutron fluence than that predicted by spherical divergence. At these ranges, the mass range is between 1.2

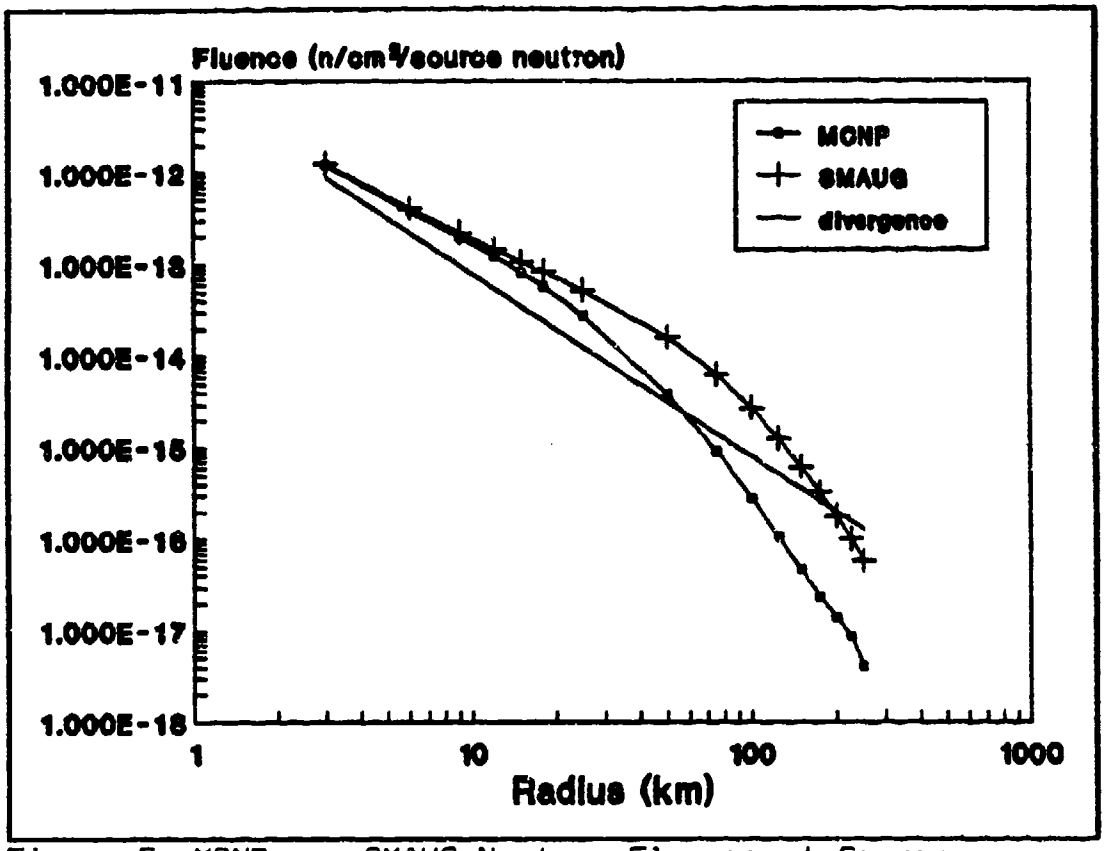

Figure 5 MCNP vs. SMAUG Neutron Fluence at Source Co-Altitude vs. Radius (Slant Range)

g/cm² at 3 kilometers and 24 g/cm² at 60 kilometers as shown in figure 6. At greater ranges (60-250 kilometers), attenuation of the neutron radiation begins to dominate over build-up. This results in a lower neutron fluence than that predicted by spherical divergence. At these ranges, the mass range is 24 g/cm² at 60 kilometers and 99.9 g/cm² at 250 kilometers. The most important transport mechanisms which account for this behavior are explained below for the MCNP results.

1) At short ranges (0-3 kilometers), the relatively low air density at this altitude leads to a small accumulated

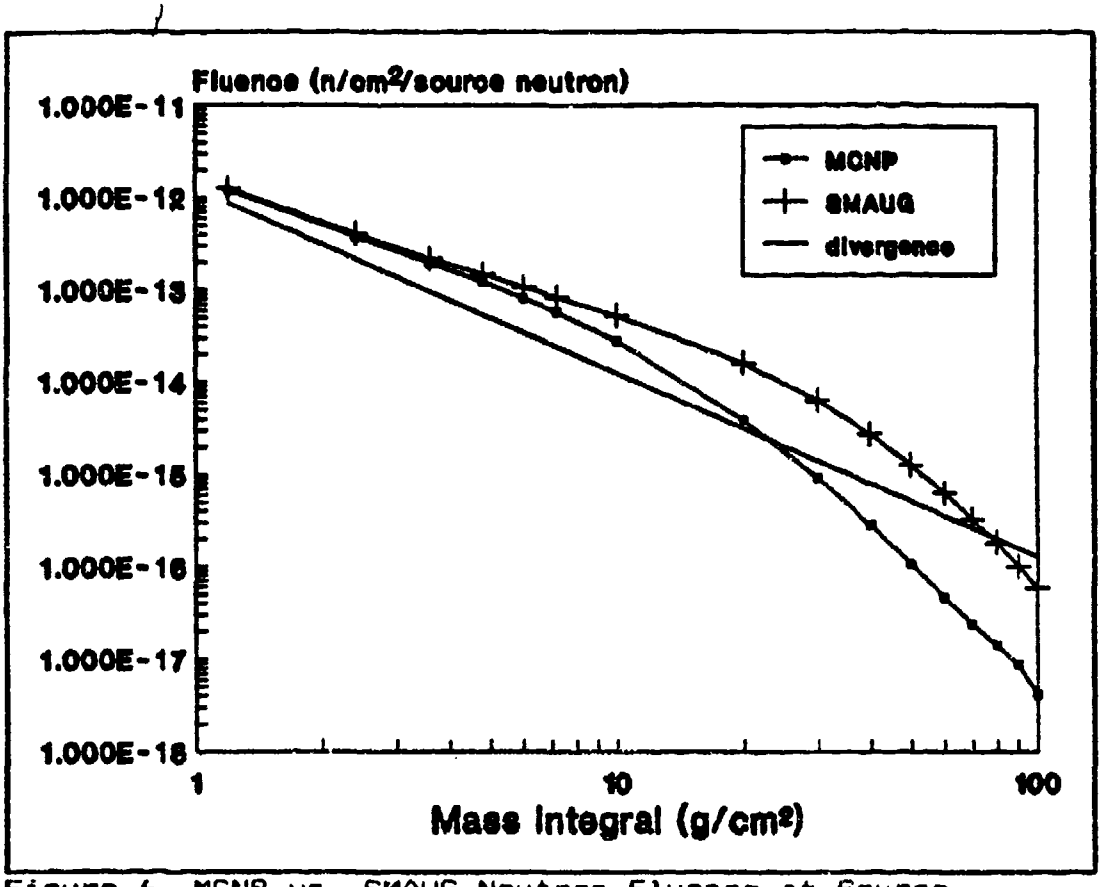

Figure 6 MCNP vs. SMAUG Neutron Fluence at Source Co-Altitude vs. Mass-Integral

mass range. Therefore, neither significant attenuation due to energy loss of the neutrons nor buildup from scattering contributions has yet occurred.

2) At intermediate ranges (3-60 kilometers), the mass range has increased to the point where buildup is occurring. In this case, the neutrons are scattering and contributing several times to the free-field fluence at the point of interest. Because the scatter cross sections for neutrons generally follow a $1/\sqrt{E}$ (1/v) relationship, the higher energy neutrons are scattering down in energy, and hence the proba-

bility for an additional scatter increases. The loss of particles due to successive scatters and their subsequent loss of energy is more than compensated for by the scattering contributions. This is the reason for the buildup at intermediate ranges.

3) At some point, the loss of neutrons due to their decreasing energy overwhelms the contribution to buildup from neutron scattering events, and attenuation begins to dominate over buildup. This occurs at ranges between 60 and 250 kilometers, where the free-field fluence just equals the value predicted by spherical divergence. The buildup factor at this point is unity. Beyond 60 kilometers, attenuation dominates over buildup from scatter because the neutrons no longer have enough energy to further contribute to the fluence via scattering contributions.

The same general trends seen in the MCNP results can be seen in the SMAUG results shown in figures 5 and 6. Close to the source, MCNP and SMAUG show good agreement. At ranges greater than about 9 kilometers, SMAUG begins to severely overpredict the neutron fluence relative to the MCNP results. Table 4 contains the ratios of SMAUG to MCNP neutron fluence results versus range along the source co-altitude band. Close to the source, the SMAUG fluence is somewhat higher, but the ratio is relatively close to 1, which confirms the accuracy of the MCNP results at close range. At 9 kilometers, SMAUG begins to overestimate the fluence signifi-

Table 4: Ratio of SMAUG to MCNP Neutron Fluence at Source Co-Altitude versus Range

Range [km]	Ratio
3	1.04
6	1.07
9	1.12
12	1.20
15	1.32
18	1.46
25	1.88
50	4.24
75	6.94
100	9.80
125	11.98
150	13.55
175	13.72
200	12.67
225	11.53
250	14.11

cantly relative to MCNP, where the ratio is 1.12. The ratios generally increase with increasing range out to a maximum ratio of 14.11 at a range of 250 kilometers. The most important reasons which account for the behavior of the SMAUG-II results are stated below.

1) SMAUG-II performs calculations of mass-integral scaling based on approximate fits to one-dimensional discrete ordinates solutions of neutron and gamma transport. Mass-integral scaling is strictly correct only in a uniform homo-

geneous medium, and works relatively well only when the mean free path of the particle is short compared to the distance over which the density varies significantly. In this analysis, the atmosphere does vary significantly in density over a relatively short vertical distance, and hence errors resulting from the mass-integral scaling approximation are expected on this basis alone.

2) The mass-integral scaling approximation used in SMAUG-II assumes that geometric divergence and scattering can be separated. Therefore, SMAUG-II would predict that the same buildup factor would exist for two detectors, one above and one below the source, provided that the slant ranges to each detector would result in both $4\pi R^2$ fluences being equal. A two-dimensional transport calculation by MCNP would predict that the radiation would undergo less buildup toward the upper detector than the lower detector. This is due to the lower air density above the source, causing fewer scatters and more particle leakage out the top of the problem, which decreases the contribution to the free-field fluence. At high altitudes, the air is tenuous and the probability for a particle escaping the problem increases because there are fewer scatters in this region. At very low altitudes, the mean free path for scatter is short, and thus the particle undergoes many scatters along its tortuous path. This results in a successive loss of particle energy. As a consequence, the particle diffuses away from the point of interest

which prevents contribution to the free-field fluence. In this case, SMAUG-II would tend to overpredict the fluence everywhere, with the overprediction becoming more severe as the mass range increases. Therefore, SMAUG-II would not be expected to account for simple particle leakage from the problem. The results shown in figure 5 shows this to be true.

The mechanism of "over the top" contribution of particles initially travelling into the upper elevations, undergoing collision, and then reflecting downward and contributing to the final result at long ranges, was not observed in these results. A mechanism of this kind is not accounted for by SMAUG, and thus if this mechanism were significant, SMAUG would tend to underestimate the fluence at these ranges. Clearly, results shown in figure 5 do not reflect this.

Overall, these results behaved in an anticipated manner, but figures 5 and 6 clearly show the deficiencies in SMAUG-II.

<u>Photon Fluence at 40 km.</u> Figure 7 shows a comparison between MCNP and SMAUG photon fluence results at an elevation of 40 kilometers (source altitude) versus radius (slant range in this case). Figure 8 shows the same results versus mass-integral. The MCNP results were computed using ring detectors and all results are normalized to one source particle. For comparison purposes, a line showing spherical

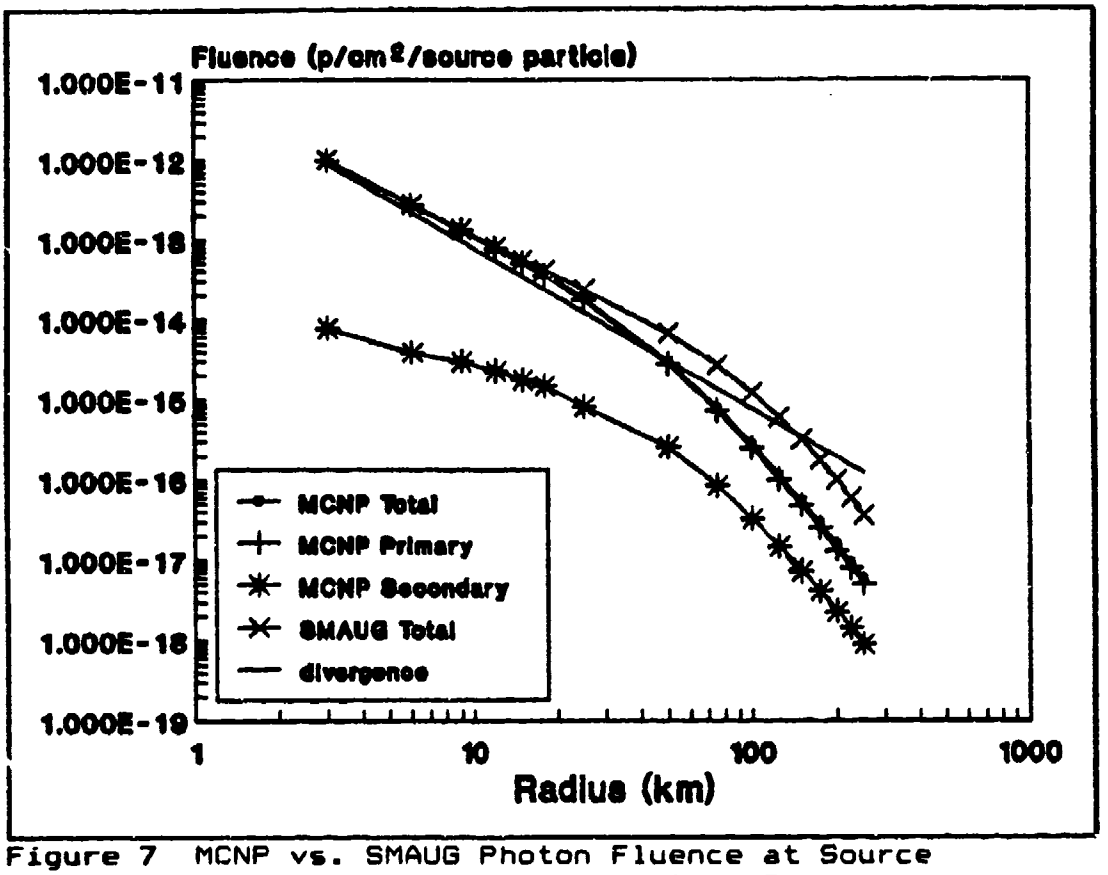

Figure 7 MCNP vs. SMAUG Photon Fluence at Source Co-Altitude vs. Radius (Slant Range)

divergence for one source particle has been plotted.

Both the primary and secondary photon fluences, computed from MCNP, have been plotted separately in order to chart the behavior of each and to see in what region each is important in contributing to the total fluence. In performing these calculations, one source (primary) photon was emitted for every source neutron emitted. This is not necessarily representative for every source; a detailed analysis to determine the optimum ratio of source photons to source neutrons was not performed due to time constraints.

Figure 7 clearly shows that the general behavior of the

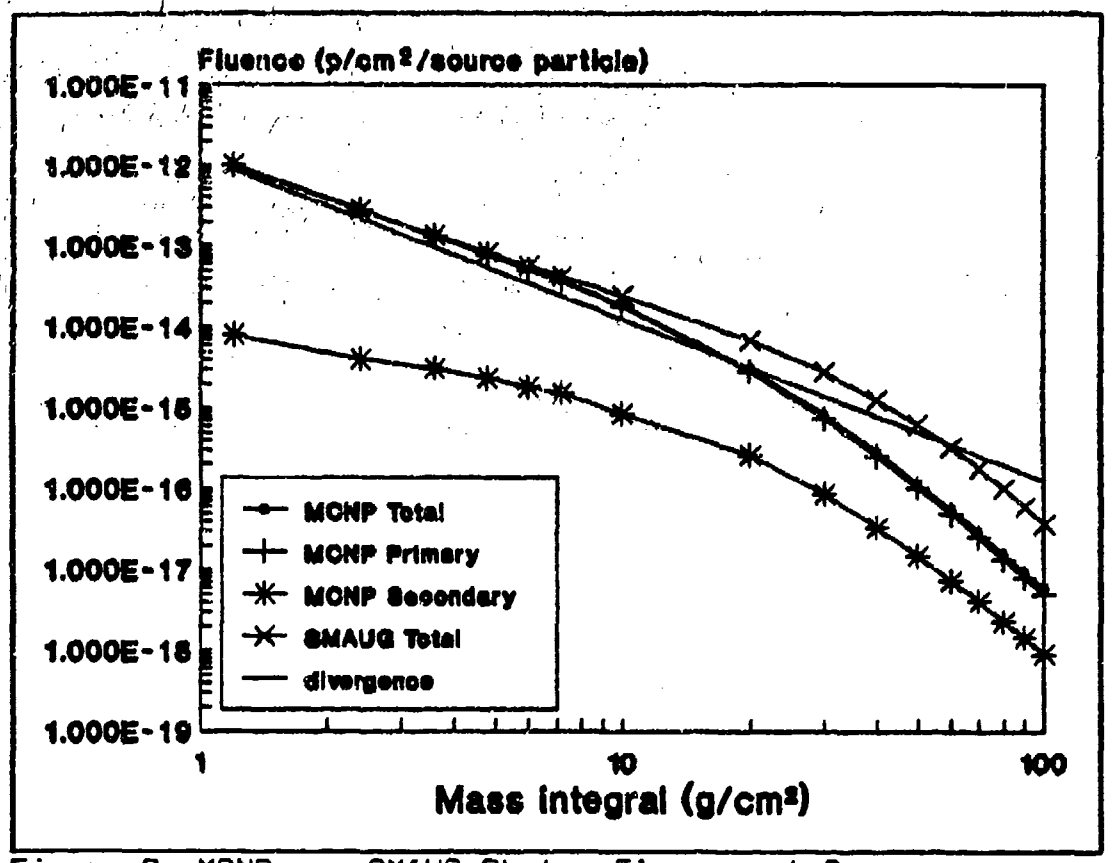

Figure 8 MCNP vs. SMAUG Photon Fluence at Source Co-Altitude vs. Mass-Integral

photon radiation generally parallels the behavior of the neutron data shown in figure 5. At ranges close to the source, the primary photon radiation exhibits a streaming nature. At intermediate ranges, buildup from primary photon scattering contributions dominates over attenuation from absorption and energy losses from scattering. Buildup in this case is less pronounced than for neutrons due to the difference in interaction mechanisms and their associated cross sections. At long ranges, attenuation dominates over buildup and the fluence is below that predicted by spherical divergence. The contribution to the free-field photon

fluence is dominated at all ranges by the primary photon radiation. Figure 7 also shows that the relative difference between the primary and secondary photons is not constant. The relative difference in fact decreases with increasing distance (mass range). Table 5 contains the ratios of SMAUG to MCNP total (primary plus secondary) photon fluence results versus range along the source co-altitude band. Close to the source, the SMAUG photon fluence agrees well with the MCNP fluence results. In this region the ratio is relatively close to 1, which confirms the accuracy of the MCNP results at close range. At 18 kilometers, SMAUG begins to over-estimate the fluence significantly relative to MCNP, where the ratio is 1.11. The ratios generally increase with increasing range out to a maximum ratio of 6.21 at a range of 250 kilometers. Reasons for the behavior of the photon radiation computed by MCNP are given below.

1) Photons interact differently than do neutrons. Photons can undergo photoelectric effect, with a cross section which varies approximately as $1/E^3$, Compton scatter, with a cross section which varies little with energy, and pair production, with a cross section which increases rapidly with increasing energy. Intuitively, differences in the transport mechanisms would be expected based on these interaction mechanisms. However, results in figure 7 show that the behavior of the photon radiation follows the same general pattern of streaming, buildup, and attenuation as the neutron

Table 5: Ratio of SMAUG to MCNP Photon Fluence at Source Co-Altitude versus Range

Range [km]	Ratio
3	1.03
6	1.01
9	1.01
12	1.03
15	1.07
18	1.11
25	1.30
50	2.25
75	3.39
100	4.45
125	5.39
150	5.88
175	6.10
200	6.60
225	6.50
250	6.21

radiation. The streaming behavior is predicted based on similar reasons given for neutron data. Both the air density and the accumulated mass range are low, therefore neither significant attenuation nor buildup from photon scattering contributions has yet occurred. Buildup occurs at intermediate ranges because both range and mass range have increased, resulting in more photon scatters which leads to multiple contributions to the free-field fluence. However, the amount of buildup is small relative to neutron buildup at

these ranges because of the nature of the energy-dependent cross sections. Once the photons have undergone a significant amount of scattering, the photon energy has dropped to the point where the $1/E^3$ photoelectric cross section dominates, and the photons are absorbed. Attenuation soon dominates over buildup at greater ranges. Attenuation in the case of the photon radiation includes attenuation from scattering as well as from absorption.

2) The magnitude of the secondary photon fluence shown in figure 7 is approximately two orders of magnitude below the magnitude of the primary photon fluence. This demonstrates that the production of a secondary photon is rare compared to the primary photon source generation rate, which is equal to the neutron source generation rate. The result is a clear dominance of the primary photon radiation at all ranges.

3) The secondary photons are generated as a result of neutron interactions with primarily nitrogen and oxygen in the atmosphere. It therefore follows that the secondary photons should be coupled in some way with the behavior of the neutron radiation. In fact, the secondary photon radiation behavior parallels the neutron radiation behavior because the neutron radiation acts like a source for the secondary photon radiation. Even though fluence data for ranges greater than 250 kilometers was not calculated, it can be inferred from the results shown in figure 7 that at very

long distances (> 250 kilometers), the secondary photon radiation would reach secular equilibrium with the neutron radiation. The reason for this is that the primary photon radiation at these distances would undergo extreme attenuation, and since the primary photon radiation is not self generating, would no longer dominate over the secondary radiation.

Neutron Fluence vs. Angle. Figure 9 is a polar plot showing the ratio of SMAUG to MCNP neutron fluence for selected source elevation angles versus slant range. The MCNP results were computed using ring detectors. The MCNP and SMAUG results were computed for ranges between 3 kilometers out to a maximum of 18 kilometers. Neutron fluence data beyond 18 kilometers was not computed because of the 60 kilometer altitude limit in computing the mass-integral in the SMAUG-II code. Because of the relatively small number of data points for each slant range versus source elevation angle combination, individual plots of fluence versus slant range are not shown. Figure 9 provides a more meaningful comparison of SMAUG performance relative to MCNP performance.

The comparison shows that SMAUG tends to overestimate the neutron fluence (except at 90 degrees) for large positive angles. For source elevation angles of 60 and 90 degrees, the SMAUG to MCNP fluence ratio tends to decrease slightly with increasing range, where the ratio is close to 1. For

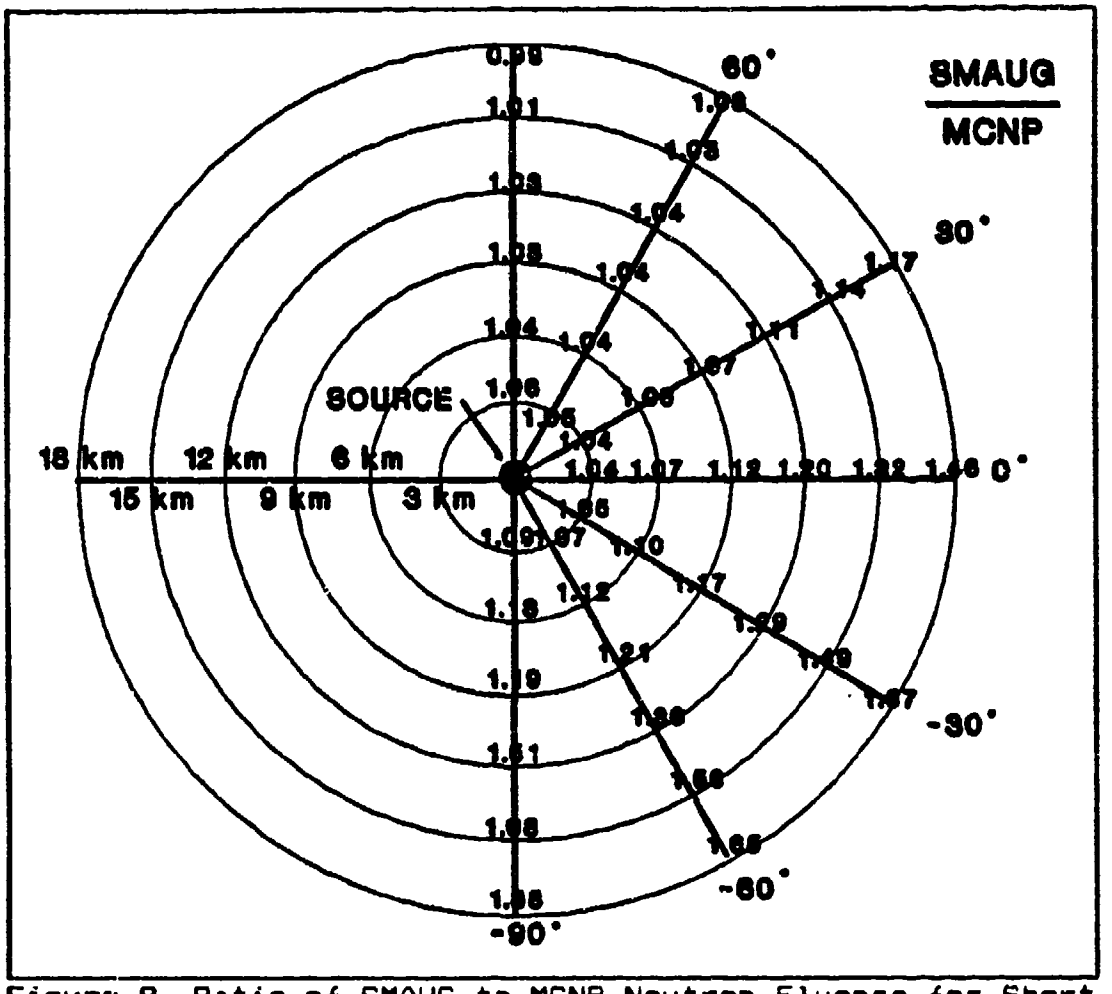

Figure 9 Ratio of SMAUG to MCNP Neutron Fluence for Short Ranges vs. Angle

source elevation angles of 30 degrees and lower, the ratios tend to increase with increasing range and decreasing angle. A maximum ratio of 1.88 is observed at a source elevation angle of -90 degrees and a slant range of 18 kilometers. The -90 degree angle and 18 kilometer range combination represents the maximum mass-integral obtainable in this plot, 74.8 g/cm^2. Figure 9 shows a definite correlation between the fluence ratios and increasing density (with

decreasing angle) and increasing mass range. Since in every case (except at 90 degrees) SMAUG overpredicts the neutron fluence, there must be one or more two-dimensional effects which reduces the neutron contribution to the free-field fluence and is not accounted for by SMAUG-II. This suggests that the mechanism of particle loss in either the upper or lower altitudes is not accounted for in SMAUG-II.

Particle loss can occur in several ways:

1) Neutron collisions leading to scatter away from the point of interest without further contribution to the fluence. A specific case of this is a particle travelling downward being scattered in the upward direction and leaving the problem without further collision.

2) Neutron collisions which lead to scatter out of the problem, i.e., the top of the atmosphere, without further collision. The probability for this mechanism increases with increasing altitude (decreasing density).

3) Successive scattering of neutrons which leads to the subsequent loss of energy. This eventually reduces the mean free path of the neutrons to a point where the neutrons diffuse away from the point of interest and can no longer contribute to the fluence. The loss mechanism that dominates depends on the altitude region (and hence the density), the direction of travel, and the initial energy of the neutrons.

The ratios shown in figure 9 suggest that SMAUG's capability to predict the neutron fluence worsens with

increasing mass-integral, especially at field points below the source altitude. This indicates that the higher air density below the source contributes to the increased attenuation by successive scattering of the neutrons and diffusion away from the point of interest. This leads to a significant loss of particles in this region. In the upper altitude regions and the largest positive angles, SMAUG's ability to predict the fluence is fairly good relative to the MCNP results. This is a consequence of the lower air density. The collision probability for neutrons is much less in the upper atmosphere than it is in the lower atmosphere. This means that most particles will have at most only a few collisions before escaping the problem.

Photon Fluence vs. Angle. Figure 10 is a polar plot showing the ratio of SMAUG to MCNP photon fluence for selected source elevation angles versus slant range. The MCNP results were computed using ring detectors for the same range and angle combinations as shown in figure 9.

The comparison shows that SMAUG tends to underestimate the photon fluence for large positive angles (except at very close range). For source elevation angles between 30 and 90 degrees, the SMAUG to MCNP fluence ratio tends to decrease with increasing range. For source elevation angles below 30 degrees, the ratios generally tend to increase with increasing range and decreasing angle. A maximum ratio of 1.74 is observed at a source elevation angle of -90 degrees and a

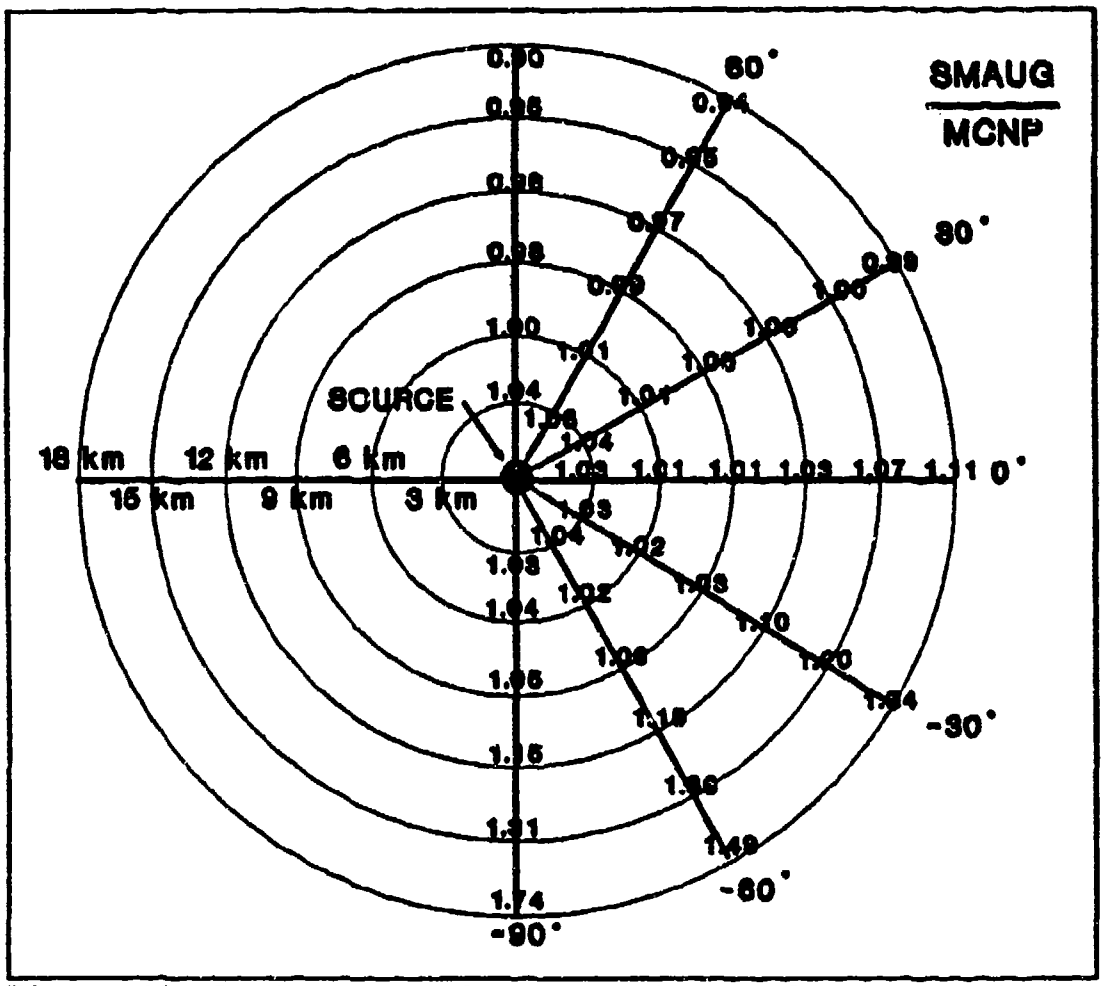

Figure 10 Ratio of SMAUG to MCNP Photon Fluence at Short Ranges vs. Angle

slant range of 18 kilometers.

The photon radiation behavior parallels the behavior of the neutron radiation at points below the source, but not above the source. If the mean free path of the photons was long compared to that of the neutrons, fewer photon scatters would occur and MCNP would predict a lower photon fluence at the point of interest relative to the neutron fluence. The raw data listed in Appendix A, corresponding to the ratios

shown in figures 9 and 10, substantiate this fact. As a consequence, photon leakage would increase as compared to the neutron leakage, especially at high altitudes.

In a comparison with SMAUG-II, the two-dimensional effects accounted for by MCNP are not accounted for by SMAUG-II. SMAUG-II fails to account for the increased particle leakage in the lower altitude regions because particles travelling downward have a high probability for collision and subsequent scatter upwards and out of the problem. This parallels the behavior of the neutron radiation. The relative differences in the SMAUG to MCNP photon ratios is less than the corresponding neutron ratios. This suggests that the two-dimensional effects which govern the behavior of the photon radiation are less pronounced than for the neutron radiation.

Computational Costs. Previous studies have demonstrated that Monte Carlo transport studies are particularly suited for cases where accurate benchmark results are needed. Computer run time has not been a critical issue because often only a few data points are needed. In terms of computer cost, Monte Carlo transport simulation has proven to be impractical compared to other methods of radiation transport such as discrete ordinates when large amounts of data are needed.

Several computer simulations using just the variable density version of MCNP were performed to provide an under-

standing of the added computational cost associated with using ring detectors versus using no ring detectors. A modified MCNP run using 80,000 source neutrons and no tallies or detectors for the 25 cell geometry shown in figure 4 was performed. Geometric splitting/Russian roulette was employed out to 180 kilometers, and a total of 573,600 particles were tracked. The run time was 153 minutes, or 0.115 seconds per source neutron. Another modified MCNP run was performed using the same geometry and number of source neutrons, but with one ring detector at a source co-altitude range of 100 kilometers. The same number of total particles were tracked. The run time was 454 minutes, or 0.341 seconds per source neutron. As a result, a run time of 301 minutes was added by using just one ring detector. An additional modified MCNP run was performed using two ring detectors at source co-altitude ranges of 125 and 150 kilometers. Again, the same total number of source particles were tracked. The run time was 655 minutes, or 0.491 seconds per source neutron. As a result, an additional 201 minutes was added to the run time by adding one more ring detector. A modified MCNP run was performed using an 18-cell geometry with 18 ring detectors for ranges out to 250 kilometers. For 100,000 source neutrons and geometric splitting, a total of 480,800 particles were tracked. The run time was 1996 minutes, or 1.2 seconds per source neutron.

A more significant basis for comparing run times is to

compare run times between the unmodified version of MCNP and the unmodified version of MCNP. Comparisons were made of run times from previous studies using ring detectors, specifically, Culp et al. [2:31-32]. An unmodified MCNP run using 7500 source neutrons and 15 ring detectors for the 181-cell geometry shown in figure 2 [2:20a] was performed. With geometric splitting/Russian roulette, a total of 380,693 particles were tracked. The run time was 580 minutes, or 4.64 seconds per source neutron. The same geometry and ring detector locations were used in a modified MCNP run. As expected, the modified version of MCNP took longer, or about 840 minutes, a 45 percent increase relative to the unmodified version of MCNP. This was a consequence of the run time added because of the array searches required in the variable density model. In reality, fewer numbers of cells would be required in the modified version of MCNP which would significantly decrease the run time.

With respect to the time-intensive array searches in the variable density model, the run times from the modified version of MCNP proved to be very competitive when the number of cells was reduced in the modified MCNP code. A comparison test was performed using the same 181-cell geometry as shown in figure 2 [2:20a]. Here, the unmodified MCNP code employed ring detectors placed at selected slant ranges from 3 to 18 kilometers for various source elevation angles. The run time results from the modified MCNP code were based on the same

geometry using only 46 cells and identical ring detector locations. The comparison test showed the modified version of MCNP ran faster than the unmodified version of MCNP by almost a factor of two. No direct run time comparisons were made using the unmodified MCNP code at radii (ground ranges) greater than 100 km. An excessive number of cells would have been required in the unmodified version of MCNP resulting in an extremely long run time.

VII. Summary and Conclusions

Summary

Validation of MCNP. Validation of the modified MCNP code was accomplished in two phases. The first phase involved validating each scale height factor for both density and mass-integral, and then validating each subroutine or function that used them. The scale height factors were used in the appropriate form of the density or mass-integral fitting equation to represent the density variation of the atmosphere. The fitting equations produced results which were within 1 percent of the reference data. The second phase involved validating the modified MCNP code as an integrated whole based on a two-part approach. In the first approach, a Monte Carlo simulation from a previous study was used to validate, on a rough basis, the results obtained from the modified MCNP code. The comparison showed a maximum relative difference in the fluence results of 2 percent. In the second approach, a simpler geometry using fine-mesh spatial grids with accurate average densities in each scale height region was incorporated into the input file. Results from the unmodified MCNP code using this input file were compared to results from the modified MCNP code. A comparison showed a maximum relative difference in the fluence results of 1 percent.

MCNP Results. Multidimensional Monte Carlo simulation studies of neutron-photon transport were performed within a

variable density atmosphere. The calculations were performed using the newly-modified version of MCNP for a point isotropic neutron-photon source at an altitude of 40 kilometers. A collection of benchmark results using ring detectors were obtained for various angles and ranges. Specifically, fluence results were obtained for field points at constant ranges as a function of angle and for field points at constant altitudes as a function of range. These results were mapped out giving fluence distribution values as a function of range and angle. The computer code SMAUG-II, which uses the mass-integral scaling approximation, was used to generate neutron and photon fluence results at the same field point locations.

Conclusions

In terms of the effort put forth, as well as the knowledge and insight gained in modifying a production Monte Carlo transport code to incorporate a variable density atmosphere, this project was a success. The limitations imposed by using discrete cells to represent the variation in air density has been eliminated. MCNP performed very well in terms of saving computer time, user overhead, and expanding the dimensions of the problem. Validation of previous studies as well as extending the body of knowledge in this area were accomplished.

Fluence data obtained with MCNP behaved in an anticipated manner, offering no particular surprises. The magnitude

of the neutron fluence was shown to be roughly an order of magnitude higher than the corresponding photon results. This indicated that neutrons were the principal form of radiation in this analysis. This also implies that the mean free path for neutron scatter was short compared to that for photons.

Along the source co-altitude band, streaming of the neutron and photon radiation was observed, indicating reduced scatter contributions at very short ranges and low mass-integral. For both neutron and photon radiation, buildup at intermediate ranges from scatter increased for decreasing source elevation angle and increasing range. The amount of buildup from the photon radiation was less pronounced than that from the neutron radiation. At long ranges, attenuation of the neutron radiation, due to successive downscatter and diffusion away from the points of interest, began to dominate over buildup, and the fluence fell off faster than predicted by spherical divergence. For the photon data, attenuation from successive scatter and absorption at low photon energies dominated buildup at longer ranges. From 3 kilometers out to at least 250 kilometers, the primary photon radiation was the principal contributor to the total coupled photon free-field fluence. It was shown that the secondary photon radiation paralleled the neutron radiation. There was evidence indicating that convergence towards secular equilibrium with the neutron radiation at very long distances (> 250 kilometers) was occurring. This served as evidence that the neutron

radiation acted as a source for the secondary photon radiation.

Listed below are several factors which influenced the MCNP results:

1) neutrons were the dominant form of radiation;

2) scattering was the dominant mechanism of neutron-photon transport within the atmosphere;

3) two-dimensional effects such as buildup, low-energy diffusion, and particle escape were primary factors in the relative differences between MCNP and SMAUG-II results.

With respect to the approximations used in this analysis, SMAUG-II predictions of neutron-photon transport characteristics were shown to be accurate to within a few percent at points within a few kilometers of the source. SMAUG-II neutron results differed by a factor of 14 along the source co-altitude band. The photon results differed by a factor of 6 at this same elevation. For ranges between 3 and 18 kilometers versus source elevation angle, SMAUG-II again showed an inability to model the two-dimensional behavior of the neutron and photon radiation as both range and mass range increased. SMAUG-II had the greatest difficulty in predicting the fluence in regions of higher density and over large mass ranges.

Based on these comparison results, there were several deficiencies noted with SMAUG-II. First, SMAUG-II could not account for the escape of particles from the problem, espe-

cially out the top. This becomes a concern at higher elevations where particle leakage can be significant because of low air density and the small probability for particle interaction. Also, leakage increased as a result of particles travelling downward, scattering upward, and leaving the problem without further collision. Second, as a direct consequence of the reasons discussed above, SMAUG-II is inadequate for use at altitudes above the original 20 kilometer limit. This stems from the inability of SMAUG-II to account for multidimensional transport effects inherent in a variable density atmosphere. This severely limits the usefulness of SMAUG-II as an initial transport diagnostic tool or as a tool for comparison against other radiation transport methods. However, this was expected since mass-integral scaling is based on one-dimensional discrete ordinates results for a homogeneous system.

Increasing the geometrical dimensions of the problem over previously used geometries in past Monte Carlo studies was now possible. The increase in run time as a consequence of incorporating a variable density atmosphere into MCNP was more than offset by the time saved in eliminating unneeded spatial cells to represent the variation of air density with altitude. An added benefit was to decrease some of the user overhead in preparing the input files.

In terms of computational costs, using ring detectors proved to be very expensive. Because of the unique nature of

the modifications, the use of cell or surface tallies became impractical. Cells were still required but were so large that average cell or surface tallies became meaningless. Using average cell or surface tallies would result in average fluence values that do not accurately represent the fluence values within a large cell, since the variation of fluence across the cell or surface is large.

In comparison to run times obtained using an unmodified version of MCNP, run times from the modified version of MCNP proved to be extremely favorable. The goal of reducing the number of cells required and at the same time offset the added run time caused by using the variable density model was accomplished. The run time added as a consequence of employing the variable density atmospheric model was more than offset by the time saved in using a small number of spatial cells.

VIII. Recommendations

The following are recommendations for further study in this area. First, more work is needed in developing the modified MCNP code so that it is applicable to a wider variety of density-dependent atmospheric transport problems. Undoubtedly, there are density-dependent parameters and capabilities employed by MCNP that were not modified in this project. Capabilities requiring modification might include fission heating within the atmosphere, radiation energy deposition, exponential transformation of the macroscopic cross section which utilizes path length stretching, and any density-dependent dose response functions. Second, an investigation of alternate geometries and/or variance reduction schemes to increase the efficiency of specific problems should be made. Third, alternative array-search algorithms might improve the efficiency of the modified MCNP code. Fourth, MCNP should be further modified to allow the use of more than one material within the atmosphere, i.e. silicon, tissue, etc. Finally, modifications to allow the user to select either the variable density version or the unmodified version should be incorporated into a single code.

Appendix A: MCNP and SMAUG Neutron and Photon Fluence Resu

MCNP vs. SMAUG Neutron Fluence at Selected Altitudes vs.

ALTITUDE = 40 km

Ground Range (km)	MCNP Neutron Fluence (n/cm²/source n)		SMAUG Fluence (n/cm²)/source n)
3	1.2046E-12	0.0158	1.2551E-12
6	3.7991E-13	0.0067	4.0831E-13
9	1.9915E-13	0.0073	2.2396E-13
12	1.2433E-13	0.0092	1.4924E-13
15	8.3064E-14	0.0084	1.0962E-13
18	5.8523E-14	0.0089	8.5201E-14
25	2.8385E-14	0.0090	5.3382E-14
50	3.8769E-15	0.0120	1.6425E-14
75	9.1952E-16	0.0187	6.3846E-15
100	2.7891E-16	0.0205	2.7332E-15
125	1.0528E-16	0.0256	1.2609E-15
150	4.5912E-17	0.0370	6.2217E-16
175	2.3697E-17	0.0624	3.2513E-16
200	1.4024E-17	0.0674	1.7764E-16
225	8.6885E-18	0.0813	1.0022E-16
250	4.0998E-18	0.0874	5.7828E-17

ALTITUDE = 60 km

Ground Range (km)	MCNP Neutron Fluence (n/cm²/source n)		SMAUG Fluence (n/cm²)/source n)
3	3.9844E-14	0.0047	3.8592E-14
6	3.7524E-14	0.0036	3.6795E-14
9	3.4411E-14	0.0035	3.4212E-14
12	3.0865E-14	0.0034	3.1255E-14
15	2.7066E-14	0.0030	2.8254E-14
18	2.3564E-14	0.0038	2.5417E-14
25	1.6532E-14	0.0035	1.9871E-14
50	4.7007E-15	0.0046	9.6673E-15
75	1.5593E-15	0.0056	5.7184E-15
100	6.2507E-16	0.0071	3.7199E-15
125	2.8793E-16	0.0078	2.5426E-15
150	1.5032E-16	0.0097	1.7896E-15
175	8.5504E-17	0.0162	1.2842E-15
200	5.0322E-17	0.0120	9.3478E-16
225	3.1846E-17	0.0153	6.8832E-16
250	2.0549E-17	0.0146	5.1194E-16

MCNP vs. SMAUG Photon Fluence at Selected Altitudes vs. Range

ALTITUDE = 40 km

Ground Range (km)	MCNP Photon Fluence Primary (p/cm²/source p)		Secondary (p/cm²/source n)		SMAUG Fluence Coupled (p/cm²)
3	9.8204E-13	0.0038	7.9830E-15	0.1120	1.0211E-12
6	2.7361E-13	0.0044	4.0190E-15	0.0442	2.8118E-13
9	1.3289E-13	0.0063	3.1097E-15	0.0589	1.3710E-13
12	7.9135E-14	0.0020	2.3603E-15	0.0376	8.3808E-14
15	5.2243E-14	0.0075	1.8363E-15	0.0355	5.7683E-14
18	3.6718E-14	0.0061	1.5446E-15	0.0356	4.2646E-14
25	1.8368E-14	0.0052	8.4712E-16	0.0541	2.4706E-14
50	2.8510E-15	0.0064	2.6109E-16	0.0596	6.9869E-15
75	7.3869E-16	0.0095	8.4884E-17	0.0464	2.7902E-15
100	2.5194E-16	0.0175	3.3049E-17	0.0395	1.2695E-15
125	1.0119E-16	0.0154	1.4741E-17	0.0452	6.2510E-16
150	4.8325E-17	0.0209	7.2322E-18	0.0508	3.2651E-16
175	2.5252E-17	0.0243	4.1083E-18	0.0783	1.7897E-16
200	1.3196E-17	0.0281	2.2770E-18	0.1204	1.0218E-16
225	7.8418E-18	0.0355	1.4547E-18	0.1221	6.0406E-17
250	5.0248E-18	0.0459	9.0242E-19	0.0987	3.6786E-17

ALTITUDE = 60 km

Ground Range (km)	MCNP Photon Fluence Primary (p/cm²/source p)		Secondary (p/cm²/source n)		SMAUG Fluence Coupled (p/cm²)
3	2.7234E-14	0.0048	6.7325E-16	0.0243	2.5517E-14
6	2.5631E-14	0.0034	6.5533E-16	0.0242	2.4105E-14
9	2.3623E-14	0.0056	6.4086E-16	0.0263	2.2094E-14
12	2.1028E-14	0.0035	6.1205E-16	0.0267	1.9822E-14
15	1.8506E-14	0.0034	5.5776E-16	0.0242	1.7553E-14
18	1.6147E-14	0.0037	5.3139E-16	0.0236	1.5447E-14
25	1.1556E-14	0.0040	4.2582E-16	0.0222	1.1461E-14
50	3.7173E-15	0.0050	1.9149E-16	0.0222	4.8070E-15
75	1.4193E-15	0.0051	8.6706E-17	0.0260	2.6133E-15
100	6.2569E-16	0.0068	4.2404E-17	0.0251	1.6254E-15
125	3.1239E-16	0.0077	2.2298E-17	0.0264	1.0877E-15
150	1.7068E-16	0.0093	1.3165E-17	0.0286	7.6103E-16
175	1.0081E-16	0.0119	8.4487E-18	0.0376	5.4851E-16
200	6.4068E-17	0.0347	5.9266E-18	0.0788	4.0390E-16
225	3.8443E-17	0.0130	3.7651E-18	0.0373	3.0235E-16
250	2.5629E-17	0.0153	2.6276E-18	0.0393	2.2935E-16

MCNP Neutron Fluence at Selected Angles vs. Range

Slant Range (km)	Elev Angle 90 Degrees (n/cm²/source n)		Elev Angle 60 Degrees (n/cm²/source n)	
3	1.1205E-12	0.0072	1.1359E-12	0.0049
6	3.3085E-13	0.0089	3.3789E-13	0.0049
9	1.6434E-13	0.0067	1.6653E-13	0.0045
12	9.7811E-14	0.0053	1.0083E-13	0.0047
15	6.6532E-14	0.0069	6.7880E-14	0.0047
18	4.8076E-14	0.0041	4.9011E-14	0.0052
25	2.7086E-14	0.0048	2.7210E-14	0.0043
50	7.7299E-15	0.0030	7.4427E-15	0.0035
75	3.6899E-15	0.0029	3.4706E-15	0.0036
100	2.1516E-15	0.0029	1.9980E-15	0.0036
125	1.4082E-15	0.0029	1.2944E-15	0.0037
150	9.8892E-16	0.0029	9.0466E-16	0.0037
175	7.3331E-16	0.0030	6.6789E-16	0.0037
200	5.6326E-16	0.0030	5.1379E-16	0.0037
225	4.4835E-16	0.0028	4.0667E-16	0.0037
250	3.6525E-16	0.0028	3.2914E-16	0.0038

Slant Range (km)	Elev Angle 30 Degrees (n/cm²/source n)		Elev Angle 0 Degrees (n/cm²/source n)	
3	1.1680E-12	0.0065	1.2046E-12	0.0158
6	3.5122E-13	0.0053	3.7991E-13	0.0067
9	1.7755E-13	0.0064	1.9915E-13	0.0073
12	1.0701E-13	0.0054	1.2433E-13	0.0092
15	7.1744E-14	0.0054	8.3064E-14	0.0084
18	5.1238E-14	0.0054	5.8523E-14	0.0089
25	2.7346E-14	0.0049	2.8385E-14	0.0090
50	6.1621E-15	0.0038	3.8769E-15	0.0120
75	2.5382E-15	0.0036	9.1952E-16	0.0187
100	1.3742E-15	0.0035	2.7891E-16	0.0205
125	8.5910E-16	0.0035	1.0528E-16	0.0256
150	5.8759E-16	0.0034	4.5912E-17	0.0370
175	4.2690E-16	0.0034	2.3697E-17	0.0624
200	3.2418E-16	0.0034	1.4024E-17	0.0674
225	2.5464E-16	0.0034	8.6885E-18	0.0813
250	2.0509E-16	0.0034	4.0998E-18	0.0874

MCNP Photon Fluence at Selected Angles vs. Range

Slant Range (km)	Elevation Angle = 90 Degrees Primary Photon (p/cm²/source p)		Secondary Photon (p/cm²/source n)	
3	9.6328E-13	0.0058	5.4849E-15	0.0817
6	2.6051E-13	0.0072	2.8701E-15	0.0607
9	1.2179E-13	0.0056	1.8464E-15	0.0609
12	7.1116E-14	0.0062	1.3756E-15	0.0486
15	4.6742E-14	0.0040	9.8375E-16	0.0316
18	3.4689E-14	0.0404	7.7951E-16	0.0300
25	1.8246E-14	0.0039	4.8104E-16	0.0046
50	5.0476E-15	0.0048	1.9205E-16	0.0257
75	2.3378E-15	0.0045	1.0260E-16	0.0219
100	1.3411E-15	0.0029	6.4421E-17	0.0222
125	8.6577E-16	0.0029	4.3465E-17	0.0220
150	6.0644E-16	0.0027	3.1421E-17	0.0234
175	4.4783E-16	0.0027	2.3698E-17	0.0226
200	3.4399E-16	0.0029	1.8624E-17	0.0219
225	2.7302E-16	0.0032	1.5330E-17	0.0204
250	2.2150E-16	0.0028	1.0637E-17	0.0204

Slant Range (km)	Elevation Angle = 60 Degrees Primary Photon (p/cm²/source p)		Secondary Photon (p/cm²/source n)	
3	9.6614E-13	0.0035	6.4555E-15	0.0854
6	2.6011E-13	0.0036	2.9231E-15	0.0472
9	1.2242E-13	0.0031	1.8989E-15	0.0440
12	7.2109E-14	0.0046	1.4052E-15	0.0344
15	4.7538E-14	0.0046	1.0611E-15	0.0306
18	3.3807E-14	0.0036	8.5263E-16	0.0391
25	1.8573E-14	0.0030	5.3234E-16	0.0038
50	5.1104E-15	0.0024	2.0247E-16	0.0227
75	2.3783E-15	0.0023	1.0272E-16	0.0206
100	1.3708E-15	0.0022	6.1986E-17	0.0206
125	8.8859E-16	0.0020	4.2257E-17	0.0205
150	6.2370E-16	0.0021	2.9772E-17	0.0204
175	4.6208E-16	0.0024	2.2368E-17	0.0209
200	3.5506E-16	0.0022	1.7544E-17	0.0211
225	2.8173E-16	0.0023	1.3799E-17	0.0202
250	2.2841E-16	0.0023	1.1369E-17	0.0277

MCNP Photon Fluence at Selected Angles vs. Range (cont)

Slant Range (km)	Elevation Angle = 30 Degrees Primary Photon (p/cm²/source p)		Secondary Photon (p/cm²/source n)	
3	9.6779E-13	0.0032	7.2728E-15	0.0862
6	2.6482E-13	0.0040	3.2906E-15	0.0454
9	1.2570E-13	0.0070	2.2524E-15	0.0372
12	7.3562E-14	0.0038	1.6658E-15	0.0330
15	4.8604E-14	0.0041	1.3008E-15	0.0323
18	3.4661E-14	0.0044	1.0721E-15	0.0349
25	1.8639E-14	0.0029	6.5318E-16	0.0336
50	4.6263E-15	0.0026	2.1450E-16	0.0276
75	2.0207E-15	0.0028	9.8811E-17	0.0250
100	1.1200E-15	0.0026	5.5391E-17	0.0215
125	7.1297E-16	0.0028	3.5090E-17	0.0210
150	4.8981E-16	0.0024	2.4437E-17	0.0209
175	3.5764E-16	0.0024	1.7813E-17	0.0213
200	2.7349E-16	0.0025	1.3491E-17	0.0209
225	2.1497E-16	0.0024	1.0655E-17	0.0214
250	1.7355E-16	0.0024	8.5805E-18	0.0220

Slant Range (km)	Elevation Angle = 0 Degrees Primary Photon (p/cm²/source p)		Secondary Photon (p/cm²/source n)	
3	9.8204E-13	0.0038	7.9830E-15	0.0954
6	2.7361E-13	0.0044	4.0190E-15	0.0442
9	1.3289E-13	0.0063	3.1097E-15	0.0589
12	7.9135E-14	0.0020	2.3603E-15	0.0376
15	5.2243E-14	0.0075	1.8363E-15	0.0355
18	3.6719E-14	0.0061	1.5446E-15	0.0356
25	1.8368E-14	0.0052	8.4379E-16	0.0586
50	2.8510E-15	0.0064	2.6109E-16	0.0596
75	7.3869E-16	0.0095	8.4884E-17	0.0464
100	2.5194E-16	0.0175	3.3049E-17	0.0395
125	1.0119E-16	0.0154	1.4741E-17	0.0452
150	4.8325E-17	0.0209	7.2322E-18	0.0508
175	2.5252E-17	0.0242	4.1083E-18	0.0783
200	1.3196E-17	0.0281	2.2770E-18	0.0877
225	7.8418E-18	0.0355	1.4547E-18	0.0961
250	5.0248E-18	0.0459	9.0242E-19	0.0987

MCNP vs. SMAUG Neutron Fluence at Short Ranges vs. Angle

Slant Range (km)	Elev Angle (Deg)	MCNP Neutron Fluence (n/cm²/source n)		SMAUG Fluence (n/cm²)/source n)
3	90	1.1205E-12	0.0072	1.1869E-12
	60	1.1359E-12	0.0049	1.1948E-12
	30	1.1680E-12	0.0065	1.2181E-12
	0	1.2046E-12	0.0158	1.2551E-12
	-30	1.2321E-12	0.0060	1.2988E-12
	-60	1.2445E-12	0.0073	1.3360E-12
	-90	1.2375E-12	0.0146	1.3509E-12
6	90	3.3085E-13	0.0089	3.4573E-13
	60	3.3789E-13	0.0049	3.5210E-13
	30	3.5122E-13	0.0053	3.7230E-13
	0	3.7991E-13	0.0067	4.0831E-13
	-30	4.1667E-13	0.0082	4.5777E-13
	-60	4.5168E-13	0.0101	5.0572E-13
	-90	4.6575E-13	0.0253	5.2637E-13
9	90	1.6434E-13	0.0067	1.6859E-13
	60	1.6653E-13	0.0045	1.7356E-13
	30	1.7755E-13	0.0064	1.9043E-13
	0	1.9915E-13	0.0073	2.2396E-13
	-30	2.3575E-13	0.0310	2.7609E-13
	-60	2.7380E-13	0.0132	3.3074E-13
	-90	2.9770E-13	0.0533	3.5437E-13
12	90	9.7811E-14	0.0053	1.0064E-13
	60	1.0083E-13	0.0047	1.0455E-13
	30	1.0701E-13	0.0054	1.1852E-13
	0	1.2433E-13	0.0092	1.4924E-13
	-30	1.5578E-13	0.0205	2.0076E-13
	-60	1.8447E-13	0.0182	2.5032E-13
	-90	1.7651E-13	0.0530	2.6681E-13
15	90	6.6532E-14	0.0069	6.6997E-14
	60	6.7880E-14	0.0047	7.0123E-14
	30	7.1744E-14	0.0054	8.1756E-14
	0	8.3064E-14	0.0084	1.0962E-13
	-30	1.0518E-13	0.0130	1.5645E-13
	-60	1.1697E-13	0.0228	1.8246E-13
	-90	1.0646E-13	0.0851	1.7878E-13
18	90	4.8076E-14	0.0041	4.7782E-14
	60	4.9011E-14	0.0052	5.0328E-14
	30	5.1238E-14	0.0054	6.0119E-14
	0	5.8523E-14	0.0089	8.5201E-14
	-30	7.3389E-14	0.0214	1.2276E-13
	-60	6.7539E-14	0.0201	1.1141E-13
	-90	4.6572E-14	0.0596	8.7739E-14

MCNP vs. SMAUG Photon Fluene at Short Ranges vs. Angle

Slant Range (km)	Elev Angle (Deg)	MCNP Photon Fluence Primary (p/cm²/source p)		MCNP Photon Fluence Secondary (p/cm²/source n)		SMAUG Fluence Coupled (p/cm²)
3	90	9.6328E-13	0.0058	5.4849E-15	0.0817	1.0040E-12
	60	9.6614E-13	0.0035	6.4555E-15	0.0854	1.0059E-12
	30	9.6779E-13	0.0032	7.2728E-15	0.0862	1.0117E-12
	0	9.8204E-13	0.0038	7.9830E-15	0.0954	1.0211E-12
	-30	9.9200E-13	0.0037	8.3638E-15	0.0731	1.0325E-12
	-60	9.9745E-13	0.0050	8.4984E-15	0.0853	1.0424E-12
	-90	1.0112E-12	0.0222	8.6136E-15	0.0975	1.0464E-12
6	90	2.6051E-13	0.0072	2.8701E-15	0.0607	2.6376E-13
	60	2.6011E-13	0.0036	2.9231E-15	0.0472	2.6550E-13
	30	2.6482E-13	0.0040	3.2906E-15	0.0454	2.7107E-13
	0	2.7361E-13	0.0044	4.0190E-15	0.0442	2.8118E-13
	-30	2.8492E-13	0.0059	5.1681E-15	0.0578	2.9525E-13
	-60	2.9692E-13	0.0074	6.9139E-15	0.0819	3.0900E-13
	-90	2.9705E-13	0.0131	6.8778E-15	0.0768	3.1494E-13
9	90	1.2179E-13	0.0056	1.8464E-15	0.0609	1.2135E-13
	60	1.2242E-13	0.0031	1.8989E-15	0.0440	1.2274E-13
	30	1.2570E-13	0.0070	2.2524E-15	0.0372	1.2751E-13
	0	1.3289E-13	0.0063	3.1097E-15	0.0589	1.3710E-13
	-30	1.4328E-13	0.0074	3.9712E-15	0.0430	1.5209E-13
	-60	1.5293E-13	0.0077	5.7999E-15	0.0605	1.6772E-13
	-90	1.6045E-13	0.0353	5.7562E-15	0.0609	1.7443E-13
12	90	7.1116E-14	0.0062	1.3756E-15	0.0486	6.9889E-14
	60	7.2109E-14	0.0046	1.4052E-15	0.0344	7.0994E-14
	30	7.3562E-14	0.0038	1.6658E-15	0.0330	7.4981E-14
	0	7.9135E-14	0.0070	2.3603E-15	0.0376	8.3808E-14
	-30	8.5504E-14	0.0067	3.9386E-15	0.0577	9.8524E-14
	-60	9.1538E-14	0.0134	6.1544E-15	0.0698	1.1240E-13
	-90	9.4749E-14	0.0529	6.5894E-15	0.0694	1.1689E-13
15	90	4.6742E-14	0.0040	9.8375E-16	0.0316	4.5461E-14
	60	4.7538E-14	0.0046	1.0611E-15	0.0306	4.6349E-14
	30	4.8604E-14	0.0041	1.3008E-15	0.0323	4.9682E-14
	0	5.2243E-14	0.0075	1.8363E-15	0.0355	5.7683E-14
	-30	5.6069E-14	0.0085	3.2330E-15	0.0427	7.0897E-14
	-60	5.4639E-14	0.0188	5.2842E-15	0.0603	7.7722E-14
	-90	5.0426E-14	0.0809	7.6478E-15	0.0988	7.6223E-14
18	90	3.4689E-14	0.0404	7.7951E-16	0.0300	3.1927E-14
	60	3.3807E-14	0.0036	8.5263E-16	0.0391	3.2653E-14
	30	3.4661E-14	0.0044	1.0721E-15	0.0349	3.5463E-14
	0	3.6718E-14	0.0061	1.5446E-15	0.0356	4.2646E-14
	-30	3.6743E-14	0.0095	2.7201E-15	0.0351	5.3056E-14
	-60	2.8615E-14	0.0156	4.1097E-15	0.0499	4.8631E-14
	-90	2.0134E-14	0.0365	3.0505E-15	0.0998	4.0410E-14

Appendix B: Sample MCNP Input File

```
+ 16NOV90 FLUENCE (RING DETECTORS) AT CO-ALTITUDE RANGES
101     1    -1.225E-3      24 -25 -23      IMP:N=1        IMP:P=1
201     1    -1.225E-3      25 -26 -23      IMP:N=1        IMP:P=1
301     1    -1.225E-3      26 -27 -23      IMP:N=1        IMP:P=1
401     1    -1.225E-3      27 -28 -1       IMP:N=1        IMP:P=1
402     1    -1.225E-3      27 -28 1 -2     IMP:N=1.21     IMP:P=1
403     1    -1.225E-3      27 -28 2 -3     IMP:N=1.44     IMP:P=1
404     1    -1.225E-3      27 -28 3 -4     IMP:N=2.4      IMP:P=1
405     1    -1.225E-3      27 -28 4 -5     IMP:N=4.08     IMP:P=1
406     1    -1.225E-3      27 -28 5 -6     IMP:N=6.75     IMP:P=1
407     1    -1.225E-3      27 -28 6 -7     IMP:N=10.3     IMP:P=2
408     1    -1.225E-3      27 -28 7 -8     IMP:N=15.54    IMP:P=2
409     1    -1.225E-3      27 -28 8 -9     IMP:N=20.6     IMP:P=3
410     1    -1.225E-3      27 -28 9 -10    IMP:N=29.85    IMP:P=3
411     1    -1.225E-3      27 -28 10 -11   IMP:N=40.6     IMP:P=3
412     1    -1.225E-3      27 -28 11 -12   IMP:N=40       IMP:P=5
413     1    -1.225E-3      27 -28 12 -13   IMP:N=58.8     IMP:P=5
414     1    -1.225E-3      27 -28 13 -14   IMP:N=89.6     IMP:P=8
415     1    -1.225E-3      27 -28 14 -15   IMP:N=318.1    IMP:P=8
416     1    -1.225E-3      27 -28 15 -16   IMP:N=340.8    IMP:P=8
417     1    -1.225E-3      27 -28 16 -17   IMP:N=449      IMP:P=10
418     1    -1.225E-3      27 -28 17 -18   IMP:N=637      IMP:P=15
419     1    -1.225E-3      27 -28 18 -19   IMP:N=1000     IMP:P=40
420     1    -1.225E-3      27 -28 19 -20   IMP:N=1        IMP:P=1
421     1    -1.225E-3      27 -28 20 -21   IMP:N=1        IMP:P=1
422     1    -1.225E-3      27 -28 21 -22   IMP:N=1        IMP:P=1
423     1    -1.225E-3      27 -28 22 -23   IMP:N=1        IMP:P=1
501     1    -1.225E-3      28 -29 -23      IMP:N=1        IMP:P=1
601     1    -1.225E-3      29 -30 -23      IMP:N=1        IMP:P=1
999     0                   23:-24:30       IMP:N=0        IMP:P=0

C       23 CONCENTRIC CYLINDERS   7 PLANES PERPEND. TO Z-AXIS
1       CZ  5E+5
2       CZ  10E+5
3       CZ  20E+5
4       CZ  30E+5
5       CZ  40E+5
6       CZ  50E+5
7       CZ  60E+5
8       CZ  70E+5
9       CZ  80E+5
10      CZ  90E+5
11      CZ  100E+5
12      CZ  120E+5
13      CZ  140E+5
14      CZ  160E+5
15      CZ  180E+5
16      CZ  200E+5
17      CZ  220E+5
```

```
18      CZ   240E+5
19      CZ   260E+5
20      CZ   280E+5
21      CZ   300E+5
22      CZ   320E+5
23      CZ   340E+5
24      PZ   0
25      PZ   15E+5
26      PZ   25E+5
27      PZ   35E+5
28      PZ   45E+5
29      PZ   60E+5
30      PZ   200E+5

MODE N P
C          ISOTROPIC NEUTRON SOURCE AT (0,0,40 klicks)
SDEF   ERG=D1 POS=0 0 40E+5 CEL=401
SC1        SOURCE SPECTRUM (GENERIC)
SI1    H 4.14E-7 1.1254E-6 3.059E-6 1.0677E-5 2.9023E-5 1.013E-4
          5.8295E-4 1.2341E-3 3.3546E-3 1.0333E-2 2.1875E-2
          2.4788E-2 5.2475E-2 0.1111 0.1576 0.5502 1.108 1.827
          2.307 2.385 3.012 4.066 4.724 4.966 6.376 7.408 8.187
          9.048 10.00 11.05 12.21 12.82 13.84 14.19
SP1    D 0 0 0 0 0 2.0226E-3 2.3974E-2
          4.2300E-2 7.9823E-2 1.1337E-1 8.4647E-2 1.4145E-2
          8.1805E-2 7.0979E-2 3.3869E-2 9.8584E-2 8.4961E-2
          6.2051E-2 2.5916E-2 3.6882E-3 2.2402E-2 2.6063E-2
          1.2918E-2 4.0545E-3 1.8073E-2 8.6953E-3 5.8951E-3
          6.1457E-3 7.8970E-3 9.4915E-3 1.6382E-2 1.7368E-2
          3.3667E-2 9.3298E-3
C           MATERIAL SPECIFICATION
M1      7014.04C  -0.78     $ CONTINUOUS NITROGEN XSEC
        8016.04C  -0.21     $ CONTINUOUS OXYGEN XSEC
        18000.01C -0.01     $ CONTINUOUS ARGON CROSS SECTION
PHYS:N   14.2               $ X-SECTIONS ABOVE 14.2 MEV EXPUNGED
C         TALLY CARDS
C         NEUTRON/PHOTON FLUENCE (RING DETECTORS) AT 250 KM
F5Z:N    40E+5 250E+5 0
F15Z:P   40E+5 250E+5 0
C
NPS    100000       $ RUN 100000 HISTORIES.
PRINT               $ PRINT ALL OUTPUT FOR EASIER DEBUGGING
```

Appendix C: Sample SMAUG-II Input/Output File Listing

Input/Output File Listing

```
PAGE   1       S M A U G - I I

     1  (title=Slant Range = 3 km at Source Co-altitude of 40 km
                              )
     2  (yield =1
                              )
     3  (read neutron
                              )
        File specification is: TNS.NEV

        (0.0           1.1315-4   9.8489-3   9.3298-3   3.3667-2
1.7368-2  1.6382-2  9.4915-3  )
        (7.8970-3    6.1457-3   5.8951-3   8.6953-3   1.8073-2
4.0545-3  1.2918-2  2.6063-2  )
        (2.2402-2    3.6882-3   2.5916-2   6.2051-2   8.4961-2
9.8584-2  3.3869-2  7.0979-2  )
        (8.1805-2    1.4145-2   8.4647-2   1.1337-1   7.9823-2
4.2300-2  2.3974-2  2.0226-3  )
        (0.0         0.0        0.0        0.0        0.0
RSIC-36 (page 71) TNS. Neut.   )
     4  (norm n=1
                              )
     5  (read gamma
                              )
        File specification is: EXP.GAM

        (1.6496-5    1.3403-4   3.0209-4   9.0754-4   2.7264-3
8.1905-3  2.4605-2  2.7044-2  )
        (4.6875-2    8.1246-2   1.4082-1   1.3014-1   1.4655-1
1.0935-1  1.2896-1  4.7940-2  )
        (3.0055-2    2.5815-2   1.5833-2   1.0701-2   1.0820-2
1.1*EXP(-1.1*En).    10Nov81.  )
     6  (norm g=1
                              )
     7  (hob=40000
                              )
     8  (alt=40000
                              )
     9  (ran=3000
                              )
    10  (go
                              )
```

Title: Slant Range = 3 km at Source Co-altitude of 40 km

Detonation yield	1.000	Terajoules.
	(.2381	Kilotons.)
Detonation altitude . .	4.0000E+04	Meters.
Prompt neutron yield . .	1.000	Neutrons.
Primary gamma yield . .	1.000	Gammas.
Receiver altitude . . .	4.0000E+04	Meters.
Receiver ground range .	3000.	Meters.
Receiver slant range . .	3000.	Meters.
Receiver air depth . . .	1.199	Grams/cm2.

A/G Cf: OFF, H-A Cf: OFF, 4-Pi: OFF.

Neutron mean energy . .	1.534	MeV.
Neutron fluence	1.2551E-12	N/cm2.
Neutron energy fluence .	1.9253E-12	MeV/CM2.
Neutron tissue dose . .	1.6992E-21	Rads(Ti).
Neutron silicon dose . .	1.6745E-22	Rads(Si).
Neutron ioniz Si dose .	1.2777E-22	Rads(Si) Ion.
1-MeV Si-equiv N fluence	7.1612E-13	N/cm2 Equiv.
Gamma mean energy . . .	.8586	MeV.
Gamma fluence	1.0211E-12	G/cm2.
Gamma energy fluence . .	8.7672E-13	MeV/cm2.
Gamma tissue dose . . .	3.9217E-22	Rads(Ti).
Gamma silicon dose . . .	3.7927E-22	Rads(Si).
Gamma air dose	4.1598E-22	Roentgens.
N+G Energy fluence . . .	2.8020E-12	MeV/cm2.
N+G Tissue dose	2.0913E-21	Rads(Ti).
N+G Silicon dose	5.4672E-22	Rads(Si).
N+G Ioniz Silicon dose .	5.0704E-22	Rads(Si) Ion.

N/G Fluence ratio . . .	1.229
N/G Energy fluence ratio	2.196
N/G Tissue dose ratio .	4.333
N/G Silicon dose ratio .	.4415

Explanation of Control Codes:

title=	Title of the problem
yield=	yield of the source (normally 1 Terrajoule)
read neutron=	read the neutron source spectrum file
norm n=	normalize neutron output results (normally 1)
read photon=	read the photon source spectrum file
norm p=	normalize photon output results (normally 1)
hob=	source height [meters]
alt=	detector altitude [meters]
ran=	detector ground range [meters]
go	run problem

Appendix D: Source Code for INTEG_MI.BAS

The following is the source code from INTEG_MI.BAS which is a Microsoft QuickBasic V4.5 computer code used to generate the mass-integral data.

```
DEFDBL A-Z
DEFINT I-L, N
DECLARE SUB SIMPSON (alt(), rho(), n, h, MI(), MI, nbegin,
nend)

'=============================================================
ver$ = "INTEG_MI.BAS version 1.1 of 23 AUG 90"
'
' written by: David L. Monti AFIT/GNE-91M for Master's Thesis
'
' This program calculates the mass integral by integrating
' a table of density values taken from the 1976 U.S. Standard
' Atmosphere Tables using a 1/3 Simpson's rule integration.
' The MI's are then tabulated as a cumulative distribution
' function of mass integral (MI) as a function of altitude.
'=============================================================

'=============================================================
'
' Variable Name      Description
' -------------      -----------
'
' alt()              array of altitude values [km]
' rho()              array of density values [g/cm^3]
' MI()               array of integrated mass integral [g/cm^2]
' delMI()            difference between adjacent mass integrals
' h                  uniform spacing between altitude values
' n                  number of data values
' nbegin             first data value in an equispaced group
' nend               last data value in an equispaced group
'
'=============================================================

CLS
PRINT #2,
"-------------------------------------------------------
----------------------"
a$   =   "###.#   ###.#   ###.##   ##.#####^^^^   ##.#####^^^^
#####.############### ##.########"

'=============================================================
'  Open data file containing reference atmospheric density
'  values
'=============================================================
```

```
OPEN "ATMOSREF.DAT" FOR INPUT AS 1

OPEN "MI.OUT" FOR OUTPUT AS 2
'=============================================================
  'Input number of density values
'=============================================================
INPUT #1, n
REDIM alt(n), rho(n), MI(0 TO n), delMI(n)

'=============================================================
  'Input altitude and density values
'=============================================================
FOR i = 1 TO n
   INPUT #1, alt(i), rho(i)
NEXT i
CLOSE #1

'=============================================================
  'Break data set into groups of constant altitude width
'=============================================================
MI = 0!
MI(0) = 0!
h = alt(2) - alt(1)       'every 50 meters
nbegin = 1
nend = 19                 'data every 50 meters up through 1 km

'=============================================================
  'Perform the 1/3 Simpson's Rule integration on group 1
'=============================================================
CALL SIMPSON(alt(), rho(), n, h, MI(), MI, nbegin, nend)

'=============================================================
  'Print to screen and print to file
'=============================================================
PRINT "integrated mass integral = "; MI * 100; "[g/cm^2]"
FOR i = nbegin TO nend STEP 2
   delMI(i) = (MI(i + 2) - MI(i)) * 100
   h = alt(i + 2) - alt(i)
   PRINT #2, USING a$; alt(i); alt(i + 2); h; rho(i); rho(i +
2); MI(i) * 100; delMI(i)
NEXT i

h = alt(22) - alt(21)     'every 100 meters
nbegin = 21               'data every 100 meters up through 5 km
nend = 59

'=============================================================
  'Perform the 1/3 Simpson's Rule integration on group 2
'=============================================================
CALL SIMPSON(alt(), rho(), n, h, MI(), MI, nbegin, nend)

PRINT "integrated mass integral = "; MI * 100; "[g/cm^2]"
```

```
FOR i = nbegin TO nend STEP 2
   delMI(i) = (MI(i + 2) - MI(i)) * 100
   h = alt(i + 2) - alt(i)
   PRINT #2, USING a$; alt(i); alt(i + 2); h; rho(i); rho(i +
2); MI(i) * 100; delMI(i)
NEXT i

h = alt(62) - alt(61)    'every 500 meters
nbegin = 61              'data every 500 meters up through 32 km
nend = 113

'=============================================================
  'Perform the 1/3 Simpson's Rule integration on group 3
'=============================================================
CALL SIMPSON(alt(), rho(), n, h, MI(), MI, nbegin, nend)

PRINT "integrated mass integral = "; MI * 100; "[g/cm^2]"
FOR i = nbegin TO nend STEP 2
   delMI(i) = (MI(i + 2) - MI(i)) * 100
   h = alt(i + 2) - alt(i)
   PRINT #2, USING a$; alt(i); alt(i + 2); h; rho(i); rho(i +
2); MI(i) * 100; delMI(i)
NEXT i

h = alt(116) - alt(115) 'every 1000 meters
nbegin = 115             'data every 1000 meters up through 200
km
nend = 281

'=============================================================
  'Perform the 1/3 Simpson's Rule integration on group 4
'=============================================================
CALL SIMPSON(alt(), rho(), n, h, MI(), MI, nbegin, nend)

PRINT "integrated mass integral = "; MI * 100; "[g/cm^2]"
FOR i = nbegin TO nend STEP 2
   delMI(i) = (MI(i + 2) - MI(i)) * 100
   h = alt(i + 2) - alt(i)
   PRINT #2, USING a$; alt(i); alt(i + 2); h; rho(i); rho(i +
2); MI(i) * 100; delMI(i)
NEXT i

h = alt(284) - alt(283)    'every 4000 meters
nbegin = 283               'data every 4000 meters up through
500 km
nend = 356

'=============================================================
  'Perform the 1/3 Simpson's Rule integration on group 5
'=============================================================
CALL SIMPSON(alt(), rho(), n, h, MI(), MI, nbegin, nend)
```

```
PRINT "integrated mass integral = "; MI * 100; "[g/cm^2]"
FOR i = nbegin TO nend STEP 2
   delMI(i) = (MI(i + 2) - MI(i)) * 100

   h = alt(i + 2) - alt(i)
   PRINT #2, USING a$; alt(i); alt(i + 2); h; rho(i); rho(i +
2); MI(i) * 100; delMI(i)
NEXT i

h = alt(359) - alt(358)   'every 5000 meters
nbegin = 358              'data every 5000 meters up through
1000 km
nend = n - 4

'=============================================================
  'Perform the 1/3 Simpson's rule integration on group 6
'=============================================================
CALL SIMPSON(alt(), rho(), n, h, MI(), MI, nbegin, nend)

PRINT "integrated mass integral = "; MI * 100; "[g/cm^2]"
FOR i = nbegin TO nend STEP 2
   delMI(i) = (MI(i + 2) - MI(i)) * 100
   h = alt(i + 2) - alt(i)
   PRINT #2, USING a$; alt(i); alt(i + 2); h; rho(i); rho(i +
2); MI(i) * 100; delMI(i)
NEXT i
CLOSE #2
END

SUB SIMPSON (alt(), rho(), n, h, MI(), MI, nbegin, nend) STATIC

'=============================================================
'
' SUBROUTINE SIMPSON:
'
' This subroutine performs a Simpson's 1/3 rule integration
' on a table of equispaced density values.
'
' Variable Name        Description
' -------------        -----------
'
'  rho()               array of density values
'  alt()               array of altitudes
'  n                   number of data values
'  h                   uniform spacing between altitude values
'  MI                  integrated mass integral
'
'=============================================================
```

```
'=============================================================
  'Integrate using three data points and step by two
  'Use 1/3 rule
'=============================================================
FOR i = nbegin TO nend STEP 2
   MI(i) = MI + (h / 3) * (rho(i) + 4 * rho(i + 1) + rho(i +
2))
   MI = MI(i)
NEXT i
END SUB
```

Appendix E: Source Codes for User-Written Subroutines/ Functions

```
      SUBROUTINE EQDIST(EDST, DTD, ZO, WO, NINP)

*=====================================================================
*
*     THIS SUBROUTINE CALCULATES 2 PARAMETERS, DEPENDING ON
*     INPUT:
*
*       1) IF THE INPUT VALUE IS THE SAMPLED DISTANCE TO
*          COLLISION FROM THE 'HSTORY.F' SUBROUTINE, THIS
*          SUBROUTINE RETURNS AN EQUIVALENT DISTANCE TO
*          COLLISION BASED ON A VARIABLE DENSITY ATMOSPHERE.
*       2) IF THE INPUT VALUE IS THE CALCULATED MEAN FREE PATH
*          FROM THE 'TRANSM.F' SUBROUTINE, THIS SUBROUTINE
*          RETURNS AN EQUIVALENT MEAN FREE PATH BASED ON A
*          VARIABLE DENSITY ATMOSPHERE.
*
*     ALL UNITS ARE IN cgs, CONSISTENT WITH MCNP.
*
*=====================================================================

*=====================================================================
*
*     THE FOLLOWING IS A LIST OF ARRAYS AND VARIABLES USED IN
*     THIS SUBROUTINE AND EXTERNAL TO THE FUNCTIONS.
*
*=====================================================================
*
*       ZO      - CURRENT PARTICLE ALTITUDE
*       WO      - Z-DIRECTION COSINE RELATIVE TO POLAR ANGLE
*       EDST    - EQUIVALENT DISTANCE TO COLLISION OR
*                 EQUIVALENT MEAN FREE PATH TO BOUNDARY/DETECTOR
*       DTD     - DISTANCE TO BOUNDARY OR DETECTOR
*       NINP    - FLAG INDICATING WHICH CALCULATIONS ARE
*                 PERFORMED
*       NR1     - NUMBER OF SCALE HEIGHT REGIONS
*
*=====================================================================
      include 'CM.inc'
      EXTERNAL MASI,DNTY,ZMAS,DMI,MIZ,EQUIVDST
      DOUBLE PRECISION ZO,ZD,WO,MICA,DENCA,DENCP,ZC
      DOUBLE PRECISION MASI,DNTY,ZMAS,DMI,MIZ,EQUIVDST,DTD
      DOUBLE PRECISION EDST,MICP,MIDA,MIINF,MIPD,MIPDH

C  DEFINE MASS INTEGRAL AT INFINITY [g/cm**2] (ZO > 990 KM)
      MIINF = 1035.63513*402448

C  DETERMINE OPTIMUM ARRAY SEARCH PARAMETERS
      L=NR1/2
      IF(WO.GE.0..AND.ZO.LT.ZI(L))THEN
```

```
            I1=1
            I2=NR1
            I3=1
         ELSEIF(WO.GE.O..AND.ZO.GE.ZI(L))THEN
            I1=L
            I2=NR1
            I3=1
         ELSEIF(WO.LT.O..AND.ZO.LT.ZI(L))THEN
            I1=L
            I2=1
            I3=-1

         ELSEIF(WO.LT.O..AND.ZO.GE.ZI(L))THEN
            I1=NR1
            I2=1
            I3=-1
         ENDIF

         IF(NINP.EQ.O)THEN

*=============================================================
C   PERFORM CALCULATIONS BASED ON INPUTS FROM 'HSTORY.F'
C     SUBROUTINE.
*=============================================================

C   CALCULATE MASS INTEGRAL ALONG PARTICLE DIRECTION IN A
C     HOMOGENEOUS SEA-LEVEL ATMOSPHERE.
            MIPDH = DMI(EDST)

C   CALCULATE MASS INTEGRAL AT CURRENT PARTICLE ALTITUDE IN
C     A VARIABLE DENSITY ATMOSPHERE.
            MICA = MASI(ZO,I1,I2,I3)

C   CALCULATE REQUIRED MASS INTEGRAL AT COLLISION ALTITUDE IN
C      A VARIABLE DENSITY ATMOSPHERE.
            MICP = MIZ(MICA, MIPDH, WO)

C   CHECK TO SEE IF COLLISION ALTITUDE IS WITHIN PROBLEM
C      LIMITS.
            IF (MICP.GE.O..AND.MICP.LE.MIINF) THEN

C   CALCULATE COLLISION ALTITUDE GIVEN REQUIRED MASS INTEGRAL
C      ALONG PARTICLE PATH.
            ZC = ZMAS(MICP,I1,I2,I3)

C   CALCULATE DENSITY AT CURRENT PARTICLE ALTITUDE AND AT
C      COLLISION ALTITUDE FOR CASES WHERE WO IS APPROXIMATELY
C      EQUAL TO O.
                  IF((ZC-ZO).LT.1000.) THEN
                     DENCA = DNTY(ZO,I1,I2,I3)
                     DENCP = DNTY(ZC,I1,I2,I3)
                  ENDIF
```

```
C  CALCULATE NEW EQUIVALENT DISTANCE TO COLLISION.
            EDST = EQUIVDST(ZC, ZO, WO, MIPDH, DENCA, DENCP)
         ELSE
            EDST = -1.
         ENDIF

      ELSEIF(NINP.EQ.1)THEN

*=============================================================
C  PERFORM CALCULATIONS BASED ON INPUTS FROM 'TRANSM.F'
C     SUBROUTINE.
*=============================================================

C  CALCULATE ALTITUDE AT DETECTOR OR BOUNDARY CROSSING.
         ZD = ZO + WO*DTD
         IF(ZD.LT.0..OR.ZD.GT.ZI(NR2))THEN
            WRITE(IUO,'(15X,A38)')MSG
            EDST=-1
            RETURN
         ENDIF

C  CALCULATE MASS-INTEGRAL ALONG PARTICLE DIRECTION IN
C    A HOMOGENEOUS ATMOSPHERE.
C    SEA-LEVEL ATMOSPHERE.
         MIPDH = DMI(DTD)

C  CALCULATE MASS INTEGRAL AT CURRENT PARTICLE ALTITUDE IN
C    A VARIABLE DENSITY ATMOSPHERE.
         MICA = MASI(ZO,I1,I2,I3)

C  CALCULATE MASS INTEGRAL AT DETECTOR/BOUNDARY ALTITUDE IN
C    A VARIABLE DENSITY ATMOSPHERE.
         MIDA = MASI(ZD,I1,I2,I3)

C  CALCULATE MASS INTEGRAL ALONG PARTICLE DIRECTION IN
C    A VARIABLE DENSITY ATMOSPHERE.
         IF (ABS(ZD-ZO).GE.1000) THEN
            MIPD = (MIDA-MICA)/WO
         ELSE
            DENCA = DNTY(ZO,I1,I2,I3)
            DENCP = DNTY(ZD,I1,I2,I3)
            MIPD = DTD*(DENCA+DENCP)/2.
         ENDIF

C  CALCULATE A NEW MEAN FREE PATH BASED ON A VARIABLE
C    DENSITY ATMOSPHERE.
         EDST = MIPDH * EDST / MIPD

       ENDIF
       RETURN
       END
```

```
      FUNCTION EQUIVDST(ZN, Z, W, MIPD, DCA, DCP)

*=======================================================================
*
C     THIS FUNCTION CALCULATES A NEW EQUIVALENT DISTANCE TO
C       COLLISION ALONG THE PARTICLE DIRECTION WHICH GIVES THE
C       SAME MASS INTEGRAL AS FOUND IN A HOMOGENEOUS SEA-LEVEL
C       ATMOSPHERE.
C
*
*=======================================================================

*=======================================================================
*
C       VARIABLES USED IN THIS FUNCTION:
C
C            ZN        - NEW ALTITUDE IN A VARIABLE DENSITY
C                        ATMOSPHERE
C            Z         - CURRENT PARTICLE ALTITUDE
C            W         - Z-DIRECTION COSINE RELATIVE TO THE
C                        POLAR ANGLE
C            DCA       - DENSITY AT CURRENT PARTICLE ALTITUDE
C            DCP       - DENSITY AT NEW ALTITUDE
C            MIPD      - MASS INTEGRAL ALONG PARTICLE DIRECTION
C                        (HOMOGENEOUS SEA-LEVEL ATMOSPHERE)
C            EQUIVDST  - EQUIVALENT DISTANCE TO COLLISION OR
C                        MEAN FREE PATH TO BOUNDARY/DETECTOR
*
*=======================================================================
      DOUBLE PRECISION ZN,Z,W,MIPD,DCA,DCP,EQUIVDST
C
C     IF THE DIFFERENCE IN ALTITUDES BECOMES SMALL ( < 10m ),
C       USE THE AVERAGE DENSITY BETWEEN THE NEW ALTITUDE AND
C       CURRENT ALTITUDE.
       IF (ABS(ZN-Z).GE.1000) THEN
          EQUIVDST = (ZN-Z)/W
       ELSE
          EQUIVDST = MIPD / (0.5*(DCA+DCP))
       ENDIF
       END
```

```
   FUNCTION MASI(Z,I1,I2,I3)

*=====================================================================
*
C      GIVEN AN ALTITUDE, FIND THE MASS INTEGRAL.
C
C      VARIABLES USED IN THIS FUNCTION:
C
C         Z     - GIVEN PARTICLE ALTITUDE
C         ZI    - ARRAY CONTAINING BASE ALTITUDE OF REGIONS
C         DENI  - ARRAY CONTAINING DENSITY AT ZI
C         AMII  - ARRAY CONTAINING MASS INTEGRAL AT ZI
C         SHFM  - ARRAY CONTAINING MASS INTEGRAL SCALE HEIGHT
C                 FACTORS
C         MASI  - MASS INTEGRAL AT GIVEN ALTITUDE
*
*=====================================================================
       include 'CM.inc'
       DOUBLE PRECISION MASI,Z
       DO 10 K=I1,I2,I3
          IF (Z.GE.ZI(K).AND.Z.LE.ZI(K+1)) THEN
            MASI =
AMII(K)+DENI(K)*SHFM(K)*(1-EXP(-(Z-ZI(K))/SHFM(K)))
          END IF
 10    CONTINUE
       END


   FUNCTION ZMAS(MI,I1,I2,I3)

*=====================================================================
*
C      GIVEN A MASS INTEGRAL, FIND THE ALTITUDE.
C
C      VARIABLES USED IN THIS FUNCTION:
C
C         MI    - GIVEN MASS INTEGRAL
C         SHFM  - ARRAY CONTAINING MASS INTEGRAL SCALE HEIGHT
C                 FACTORS
C         ZI    - ARRAY CONTAINING BASE ALTITUDE OF REGIONS
C         AMII  - ARRAY CONTAINING MASS INTEGRAL AT ZI
C         DENI  - ARRAY CONTAINING DENSITY AT ZI
C         ZMAS  - ALTITUDE CORRESPONDING TO GIVEN MASS INTEGRAL
*
*=====================================================================
       include 'CM.inc'
       DOUBLE PRECISION MI,ARG,ZMAS
       DO 30 K=I1,I2,I3
          IF (MI.GE.AMII(K).AND.MI.LE.AMII(K+1)) THEN
             ARG = LOG(1 + (AMII(K) - MI) / (DENI(K) *
SHFM(K)))
             ZMAS = ZI(K) - SHFM(K) * ARG
```

```
         END IF
30    CONTINUE
      END

   FUNCTION DNTY(Z,I1,I2,I3)

*=================================================================
*
C     GIVEN AN ALTITUDE, FIND THE DENSITY.
C
C     VARIABLES USED IN THIS FUNCTION:
C
C          Z    - GIVEN PARTICLE ALTITUDE
C          ZI   - ARRAY CONTAINING BASE ALTITUDE OF REGIONS
C          DENI - ARRAY CONTAINING DENSITY AT ZI
C          SHFD - ARRAY CONTAINING DENSITY SCALE HEIGHT
C                 FACTORS
C          DNTY - DENSITY CORRESPONDING TO GIVEN ALTITUDE
*
*=================================================================
      include 'CM.inc'
      DOUBLE PRECISION Z,DNTY
      DO 10 K=I1,I2,I3
         IF (Z.GE.ZI(K).AND.Z.LE.ZI(K+1)) THEN
            DNTY = DENI(K) * EXP(-(Z-ZI(K)) / SHFD(K))
         END IF
10    CONTINUE
      END

   FUNCTION DMI(DIST)

*=================================================================
*
C     CALCULATE MASS INTEGRAL BETWEEN TWO POINTS IN A
C     SEA-LEVEL HOMOGENEOUS ATMOSPHERE.
C
C     VARIABLES USED IN THIS FUNCTION:
C
C          DIST - DISTANCE TO COLLISION OR MEAN FREE PATH TO
C                 BOUNDARY/DETECTOR
C          DMI  - MASS INTEGRAL ALONG PARTICLE DIRECTION
*
*=================================================================
      DOUBLE PRECISION DIST,DMI
C
C  CALCULATE MASS INTEGRAL ALONG PARTICLE PATH.
         DMI = 1.225E-3*DIST
      END

   FUNCTION MIZ(MIP, DMI, W)
```

```
      FUNCTION MIZ(MIP, DMI, W)

*=====================================================================
*
C     CALCULATE MASS INTEGRAL AT NEW ALTITUDE IN AN EXPONENTIAL
C       ATMOSPHERE.
C
C       VARIABLES USED IN THIS FUNCTION:
C
C            MIP - MASS INTEGRAL AT CURRENT PARTICLE ALTITUDE
C                  IN A VARIABLE DENSITY ATMOSPHERE
C            DMI - MASS INTEGRAL ALONG PARTICLE DIRECTION IN A
C                  HOMOGENEOUS SEA-LEVEL ATMOSPHERE
C            W   - Z-DIRECTION COSINE RELATIVE TO THE POLAR
C                  ANGLE
C            MIZ - MASS INTEGRAL AT NEW ALTITUDE IN A
C                  VARIABLE DENSITY ATMOSPHERE
*
*=====================================================================
      DOUBLE PRECISION MIP,DMI,W,MIZ
C
C     CALCULATE MASS INTEGRAL AT NEW ALTITUDE.
      MIZ = W*DMI + MIP
      END


      BLOCK DATA ATINIT

*=====================================================================
*
C       THIS DATA BLOCK IS USED TO SUPPORT THE VARIABLE
C       DENSITY ATMOSPHERIC MODEL.  INITIALIZE COMMON /ATMCOM/
C       WITH VALUES OF ATMOSPHERIC PARAMETERS.
*
*=====================================================================
      include 'CM.inc'
*=====================================================================
*
C          SHFM - ARRAY CONTAINING MASS INTEGRAL SCALE HEIGHT
C                 FACTORS
C          SHFD - ARRAY CONTAINING DENSITY SCALE HEIGHT FACTORS
C          ZI   - ARRAY CONTAINING BASE ALTITUDE OF VERTICAL
C                 REGIONS
C          DENI - ARRAY CONTAINING DENSITY AT ZI
C          AMII - ARRAY CONTAINING MASS INTEGRAL AT ZI
*
*=====================================================================
*
      DATA SHFM/1034124.022372781,1009981.924149543,
     1          986693.172619466,964503.5327215038,
     2          941155.9145785341,888092.312585042,
     3          692868.8443723,637442.9797604,
```

```
     4           626192.9959628,639736.90617414,
     5           47557.78050254,710362.4275112881,
     6           838211.2645959415,776503.932153373,
     7           683277.3511724839,612608.5454716644,
     8           557270.926150725,568864.8492265636,
     9           619813.9513853799,935109.6091771976,
     +           1267217.415038409,1578526.59297959,
     +           1870150.85627943,2219020.933057442,
     +           2714282.134795458,3257224.61137614,
     +           3991584.358044663,4584848.61083246,
     +           5162659.761537237,5791446.057543592,
     +           5501266.555948576,6836368.561027177,
     +           7834040.063075421,9814372.605576273,
     +           13917805.4965649,18877525.61508398/
      DATA SHFD/1030391.726068488,1006927.055016296,
     1           983153.5607496358,960534.1411264988,
     2           937232.106253662,866352.1969023093,
     3           664086.7633898156,637638.46529,
     4           627630.265119,642604.7540969,
     5           654589.3995756,736011.6057506185,
     6           834195.106975831,758287.3616637037,
     7           666098.102745308,592758.5281268486,
     8           553227.4697274631,570413.0947863342,
     9           678176.4068898259,997277.941535646,
     +           1324262.260093013,1632165.675462571,
     +           1919412.5389299,2313392.496297635,
     +           2797412.470495623,3408285.286706647,
     +           4112545.885579616,4680457.552711085,
     +           5311463.853509105,5890652.50294756,
     +           6360111.158318114,6989325.564711994,
     +           8162740.323944079,10419949.4345468,
     +           14188168.29614109,19869924.24084625/
      DATA ZI/0.,1.D+5,2.D+5,3.D+5,4.D+5,5.D+5,1.D+6,
     1         1.5D+6,2.D+6,2.5D+6,3.D+6,4.D+6,5.D+6,
     2         6.D+6,7.D+6,8.D+6,9.D+6,1.D+7,1.1D+7,
     3         1.2D+7,1.3D+7,1.4D+7,1.5D+7,1.6D+7,1.8D+7,
     4         2.0D+7,2.4D+7,2.8D+7,3.2D+7,4.0D+7,4.8D+7,
     5         5.6D+7,6.4D+7,7.2D+7,8.0D+7,8.8D+7,9.9D+7/
      DATA DENI/1.225D-3,1.1117D-3,1.0066D-3,9.0925D-4,
     1          8.1935D-4,7.3643D-4,4.1351D-4,1.9476D-4,
     2          8.891D-5,4.0084D-5,1.841D-5,3.9957D-6,
     3          1.0269D-6,3.0968D-7,8.2829D-8,1.8458D-8,
     4          3.416D-9,5.604D-10,9.708D-11,2.222D-11,
     5          8.152D-12,3.831D-12,2.076D-12,1.233D-12,
     6          5.194D-13,2.541D-13,7.858D-14,2.971D-14,
     7          1.264D-14,2.803D-15,7.208D-16,2.049D-16,
     8          6.523D-17,2.448D-17,1.136D-14,6.464D-18,
     9          3.716D-18/
      DATA AMII/0.,116.7635,222.607167,318.334333,
     1          404.704533,482.4368,763.994467,911.2723,
     2          978.75726666666669,1009.379620,
     3          1023.286286666667,1032.662946666667,
```

```
     4          1034.806793333334,1035.406480000001,
     5          1035.580609766667,1035.624107866667,
     6          1035.633205146667,1035.634792366667,
     7          1035.635056196001,1035.635104380667,
     8          1035.635118027400,1035.635123665300,
     9          1035.635126503134,1035.635128111100,
     +          1035.635129736200,1035.635130471237,
     +          1035.635131056504,1035.635131255017,
     +          1035.635131334304,1035.635131385704,
     +          1035.635131397859,1035.635131400898,
     +          1035.635131401864,1035.635131402191,
     +          1035.635131402325,1035.635131402394,
     +          1035.635131402448/
C
      END
```

Appendix F: Neutron and Gamma Spectrum Energy Groups

Neutron Spectrum Energy Groups

Group	Energy Band [MeV]
1	16.91 to 19.64
2	14.92 to 16.91
3	14.19 to 14.92
4	13.84 to 14.19
5	12.82 to 13.84
6	12.21 to 12.82
7	11.05 to 12.21
8	10.00 to 11.05
9	9.048 to 10.00
10	8.187 to 9.048
11	7.408 to 8.187
12	6.376 to 7.408
13	4.966 to 6.376
14	4.724 to 4.966
15	4.066 to 4.724
16	3.012 to 4.066
17	2.385 to 3.012
18	2.307 to 2.385
19	1.827 to 2.307
20	1.108 to 1.827
21	0.5502 to 1.108
22	0.1576 to 0.5502
23	0.1111 to 0.1576
24	5.2475E-2 to 0.1111
25	2.4788E-2 to 5.2475E-2
26	2.1875E-2 to 2.4788E-2
27	1.0333E-2 to 2.1875E-2

Neutron Spectrum Energy Groups (Cont)

Group	Energy Band [MeV]		
28	3.3546E-3	to	1.0333E-2
29	1.2341E-3	to	3.3546E-2
30	5.8295E-4	to	1.2341E-3
31	1.0130E-4	to	5.8295E-4
32	2.9023E-5	to	1.0130E-4
33	1.0677E-5	to	2.9023E-5
34	3.0590E-6	to	1.0677E-5
35	1.1254E-6	to	3.0590E-6
36	4.1400E-7	to	1.1254E-6
37	1.0000E-11	to	4.1400E-7

Photon Spectrum Energy Groups

Group	Energy Band [MeV]
1	10.00 to 14.00
2	8.00 to 10.00
3	7.00 to 8.00
4	6.00 to 7.00
5	5.00 to 6.00
6	4.00 to 5.00
7	3.00 to 4.00
8	2.50 to 3.00
9	2.00 to 2.50
10	1.50 to 2.00
11	1.00 to 1.50
12	0.70 to 1.00
13	0.45 to 0.70
14	0.30 to 0.45
15	0.15 to 0.30
16	0.10 to 0.15
17	7.00E-2 to 0.10
18	4.50E-2 to 7.00E-2
19	3.00E-2 to 4.50E-2
20	2.00E-2 to 3.00E-2
21	1.00E-2 to 2.00E-2

Bibliography

1. Shulstad, Raymond A. Capt, USAF. An Evaluation of Mass Integral Scaling as Applied to the Atmospheric Radiation Transport, Doctoral Dissertation, Air Force Institute of Technology (AU), DS/PH/76-3, November 1976.

2. Culp, Donald R., Capt. et al. "Monte Carlo Simulation of Atmospheric Neutron Transport at High Altitudes Using MCNP", Technical Report AFIT/EN-TR-90-5, School of Engineering, Air Force Institute of Technology, (AU), Wright-Patterson AFB, OH. August 1990.

3. Murphy, Harry M. "A User's Guide to the SMAUG-II Computer Code", Air Force Weapon's Laboratory, Kirtland AFB, NM. 4 March 1981.

4. RSIC Computer Code Collection CCC-200. "MCNP Version 3B, Monte Carlo Neutron and Photon Transport System", Contributed by Los Alamos National Laboratory. March 1989.

5. U.S. Standard Atmosphere, 1976. Washington, D.C.: U.S. Government Printing Office, October 1976.

6. Booth, Thomas E. "A Sample Problem for Variance Reduction in MCNP", Los Alamos Publication LA-10363-MS, Los Alamos National Laboratory, NM. October 1985.

7. Monti, David L., Capt. "Modifications to MCNP, Version 3B: Incorporating a Variable Density Atmosphere", Technical Report AFIT/EN-TR-91-2, School of Engineering, Air Force Institute of Technology (AU), Wright-Patterson AFB, OH. March 1991.

8. Gerald, Curtis F. and Patrick O. Wheatly. Applied Numerical Analysis, (third Edition). San Luis Obispo, CA: Addison-Wesley, October 1984.

Vita

Captain David L. Monti was born on 16 December 1959 in Shreveport, Louisiana. He attended his last year of High School in 1977. He enlisted in the United States Air Force in September 1978. After basic training, he was assigned to the 2852nd Air Base Group, McClellan Air Force Base, California, and then to the 20th Organizational Maintenance Squadron, RAF Upper Heyford, England, and then to the 4450th Tactical Group, Nellis AFB, Nevada. He served as an aircraft crew chief on F-111 A/D/E/F, F-4E, F-5E, F-106A, A-10, T-39A, and F-117 aircraft. He was accepted into the Airman's Education and Commissioning Program (AECP) in January 1983 and received a Bachelor of Science Degree in Nuclear Engineering from Texas A&M University in 1986. He was commissioned a Second Lieutenant in the Air Force in the winter of 1986. After commissioning, he was assigned to the Air Force Technical Applications Center (AFTAC), Technical Operations Division, McClellan AFB, California, where he was assigned as Chief Project Officer, Gas Analysis Laboratory. He entered the Nuclear Engineering Program at the Air Force Institute of Technology in August of 1989.

Permanent Address: None

REPORT DOCUMENTATION PAGE

Form Approved
OMB No. 0704-0188

1. AGENCY USE ONLY (Leave blank)	2. REPORT DATE	3. REPORT TYPE AND DATES COVERED
	March 1991	Master's Thesis

4. TITLE AND SUBTITLE
HIGH ALTITUDE NEUTRAL PARTICLE TRANSPORT USING THE MONTE CARLO SIMULATION CODE MCNP WITH VARIABLE DENSITY ATMOSPHERE

5. FUNDING NUMBERS

6. AUTHOR(S)
David L. Monti, Captain, USAF

7. PERFORMING ORGANIZATION NAME(S) AND ADDRESS(ES)
Air Force Institute of Technology, WPAFB, OH 45433-6583

8. PERFORMING ORGANIZATION REPORT NUMBER
AFIT/GNE/ENP/91M-6

9. SPONSORING/MONITORING AGENCY NAME(S) AND ADDRESS(ES)

10. SPONSORING/MONITORING AGENCY REPORT NUMBER

11. SUPPLEMENTARY NOTES

12a. DISTRIBUTION/AVAILABILITY STATEMENT
Approved for public release; distribution unlimited

12b. DISTRIBUTION CODE

13. ABSTRACT (Maximum 200 words) The Monte Carlo transport code, MCNP was modified for purposes of two-dimensional neutron-photon transport modelling in a variable density atmosphere. Calculations were performed using cylindrical (r,z) geometry and a point isotropic neutron-photon source at an elevation of 40 kilometers. Neutron and photon fluence results were computed using ring detectors for field points at constant range versus source elevation angle and for field points at constant altitude versus radius. Comparisons between the modified and unmodified versions of MCNP showed a decrease in run time by a factor of two was possible. Only a fraction of the spatial cells previously required were used. Results showed streaming of the neutron and photon radiation at very close ranges. Buildup from multiple scattering contributions proved to be the dominant effect at intermediate ranges. Attenuation from successive downscatter in energy was shown to be the dominant effect at ranges greater than about 60 kilometers. Results obtained with MCNP were compared to those obtained with the computer code SMAUG-II, which uses the mass-integral scaling approximation. The comparison showed SMAUG-II to be accurate at points close to the source, but serious errors were encountered at ranges exceeding 9 kilometers as the mass range increased.

14. SUBJECT TERMS	15. NUMBER OF PAGES
Radiation Transport, Variable Density Atmosphere, Neutron-Photon Transport, Monte Carlo Simulation	135
	16. PRICE CODE

17. SECURITY CLASSIFICATION OF REPORT	18. SECURITY CLASSIFICATION OF THIS PAGE	19. SECURITY CLASSIFICATION OF ABSTRACT	20. LIMITATION OF ABSTRACT
Unclassified	Unclassified	Unclassified	Unlimited

GENERAL INSTRUCTIONS FOR COMPLETING SF 298

The Report Documentation Page (RDP) is used in announcing and cataloging reports. It is important that this information be consistent with the rest of the report, particularly the cover and title page. Instructions for filling in each block of the form follow. It is important to ***stay within the lines*** to meet ***optical scanning requirements***.

Block 1. Agency Use Only *(Leave blank)*.

Block 2. Report Date. Full publication date including day, month, and year, if available (e.g. 1 Jan 88). Must cite at least the year.

Block 3. Type of Report and Dates Covered. State whether report is interim, final, etc. If applicable, enter inclusive report dates (e.g. 10 Jun 87 - 30 Jun 88).

Block 4. Title and Subtitle. A title is taken from the part of the report that provides the most meaningful and complete information. When a report is prepared in more than one volume, repeat the primary title, add volume number, and include subtitle for the specific volume. On classified documents enter the title classification in parentheses.

Block 5. Funding Numbers. To include contract and grant numbers; may include program element number(s), project number(s), task number(s), and work unit number(s). Use the following labels:

C	- Contract	**PR**	- Project
G	- Grant	**TA**	- Task
PE	- Program Element	**WU**	- Work Unit Accession No.

Block 6. Author(s). Name(s) of person(s) responsible for writing the report, performing the research, or credited with the content of the report. If editor or compiler, this should follow the name(s).

Block 7. Performing Organization Name(s) and Address(es). Self-explanatory.

Block 8. Performing Organization Report Number. Enter the unique alphanumeric report number(s) assigned by the organization performing the report.

Block 9. Sponsoring/Monitoring Agency Name(s) and Address(es). Self-explanatory.

Block 10. Sponsoring/Monitoring Agency Report Number. *(If known)*

Block 11. Supplementary Notes. Enter information not included elsewhere such as: Prepared in cooperation with...; Trans. of...; To be published in.... When a report is revised, include a statement whether the new report supersedes or supplements the older report.

Block 12a. Distribution/Availability Statement. Denotes public availability or limitations. Cite any availability to the public. Enter additional limitations or special markings in all capitals (e.g. NOFORN, REL, ITAR).

- **DOD** - See DoDD 5230.24, "Distribution Statements on Technical Documents."
- **DOE** - See authorities.
- **NASA** - See Handbook NHB 2200.2.
- **NTIS** - Leave blank.

Block 12b. Distribution Code.

- **DOD** - Leave blank.
- **DOE** - Enter DOE distribution categories from the Standard Distribution for Unclassified Scientific and Technical Reports.
- **NASA** - Leave blank.
- **NTIS** - Leave blank.

Block 13. Abstract. Include a brief *(Maximum 200 words)* factual summary of the most significant information contained in the report.

Block 14. Subject Terms. Keywords or phrases identifying major subjects in the report.

Block 15. Number of Pages. Enter the total number of pages.

Block 16. Price Code. Enter appropriate price code *(NTIS only)*.

Blocks 17. - 19. Security Classifications. Self-explanatory. Enter U.S. Security Classification in accordance with U.S. Security Regulations (i.e., UNCLASSIFIED). If form contains classified information, stamp classification on the top and bottom of the page.

Block 20. Limitation of Abstract. This block must be completed to assign a limitation to the abstract. Enter either UL (unlimited) or SAR (same as report). An entry in this block is necessary if the abstract is to be limited. If blank, the abstract is assumed to be unlimited.